Lawrence Berkeley National Laboratory

Title
PETROLOGY AND RADIOGEOLOGY OF THE STRIPA PLUTON

Permalink
https://escholarship.org/uc/item/8h50x591

Author
Wollenberg, Harold

Publication Date
1980-12-01

SWEDISH-AMERICAN COOPERATIVE PROGRAM ON RADIOACTIVE WASTE STORAGE IN MINED CAVERNS IN CRYSTALLINE ROCK

PETROLOGY AND RADIOGEOLOGY OF THE STRIPA PLUTON

Harold Wollenberg, Steve Flexser,
and Lennart Andersson

Lawrence Berkeley Laboratory
University of California
Berkeley, California 94720

December 1980

A Joint Project of

DISCLAIMER

This document was prepared as an account of work sponsored by the United States Government. While this document is believed to contain correct information, neither the United States Government nor any agency thereof, nor the Regents of the University of California, nor any of their employees, makes any warranty, express or implied, or assumes any legal responsibility for the accuracy, completeness, or usefulness of any information, apparatus, product, or process disclosed, or represents that its use would not infringe privately owned rights. Reference herein to any specific commercial product, process, or service by its trade name, trademark, manufacturer, or otherwise, does not necessarily constitute or imply its endorsement, recommendation, or favoring by the United States Government or any agency thereof, or the Regents of the University of California. The views and opinions of authors expressed herein do not necessarily state or reflect those of the United States Government or any agency thereof or the Regents of the University of California.

PETROLOGY AND RADIOGEOLOGY OF THE STRIPA PLUTON

Harold Wollenberg, Steve Flexser, and Lennart Andersson

Earth Sciences Division
Lawrence Berkeley Laboratory
University of California
Berkeley, California 94720

December, 1980

PREFACE

This report is one of a series documenting the results of the Swedish-American cooperative research program in which the cooperating scientists explore the geological, geophysical, hydrological, geochemical, and structural effects anticipated from the use of a large crystalline rock mass as a geologic repository for nuclear waste. This program has been sponsored by the Swedish Nuclear Power Utilities through the Swedish Nuclear Fuel Supply Company (SKBF), and the U.S. Department of Energy (DOE) through the Lawrence Berkeley Laboratory.

The principal investigators are L.B. Nilsson and O. Degerman for SKBF, and N.G.W. Cook, P.A. Witherspoon, and J.E. Gale for LBL. Other participants will appear as authors of the individual reports.

Previous technical reports in this series are listed below.

1. Swedish-American Cooperative Program on Radioactive Waste Storage in Mined Caverns by P.A. Witherspoon and O. Degerman. (LBL-7049, SAC-01).

2. Large Scale Permeability Test of the Granite in the Stripa Mine and Thermal Conductivity Test by Lars Lundstrom and Haken Stille. (LBL-7052, SAC-02).

3. The Mechanical Properties of the Stripa Granite by Graham Swan. (LBL-7074, SAC-03).

4. Stress Measurements in the Stripa Granite by Hans Carlsson. (LBL-7078, SAC-04).

5. Borehole Drilling and Related Activities at the Stripa Mine by P.J. Kurfurst, T. Hugo-Persson, and G. Rudolph. (LBL-7080, SAC-05).

6. A Pilot Heater Test in the Stripa Granite by Hans Carlsson. (LBL-7086, SAC-06).

7. An Analysis of Measured Values for the State of Stress in the Earth's Crust by Dennis B. Jamison and Neville G.W. Cook. (LBL-7071, SAC-07).

8. Mining Methods Used in the Underground Tunnels and Test Rooms at Stripa by B. Andersson and P.A. Halen. (LBL-7081, SAC-08).

9. Theoretical Temperature Fields for the Stripa Heater Project by T. Chan, Neville G.W. Cook, and C.F. Tsang. (LBL-7082, SAC-09).

10. Mechanical and Thermal Design Considerations for Radioactive Waste Repositories in Hard Rock. Part I: An Appraisal of Hard Rock for Potential Underground Repositories of Radioactive Waste by N.G.W. Cook; Part II: In Situ Heating Experiments in Hard Rock: Their Objectives and Design by N.G.W. Cook and P.A. Witherspoon. (LBL-7073, SAC-10).

11. Full-Scale and Time-Scale Heating Experiments at Stripa: Preliminary Results by N.G.W. Cook and M. Hood. (LBL-7072, SAC-11).

12. Geochemistry and Isotope Hydrology of Groundwaters in the Stripa Granite: Results and Preliminary Interpretation by P. Fritz, J.F. Barker, and J.E. Gale. (LBL-8285, SAC-12).

13. Electrical Heaters for Thermo-Mechanical Tests at the Stripa Mine by R.H. Burleigh, E.P. Binnall, A.O. DuBois, D.O. Norgren, and A.R. Ortiz. (LBL-7063, SAC-13).

14. Data Acquisition, Handling, and Display for the Heater Experiments at Stripa by Maurice B. McEvoy. (LBL-7063, SAC-14).

15. An Approach to the Fracture Hydrology at Stripa: Preliminary Results by J.E. Gale and P.A. Witherspoon. (LBL-7079, SAC-15).

16. Preliminary Report on Geophysical and Mechanical Borehole Measurements at Stripa by P. Nelson, B. Paulsson, R. Rachiele, L. Andersson, T. Schrauf, W. Hustrulid, O. Duran, and K.A. Magnussen. (LBL-8280, SAC-16).

17. Observations of a Potential Size-Effect in Experimental Determination of the Hydraulic Properties of Fractures by P.A. Witherspoon, C.H. Amick, J.E. Gale, and K. Iwai. (LBL-8571, SAC-17).

18. Rock Mass Characterization for Storage in Nucler Waste in Granite by P.A. Witherspoon, P. Nelson, T. Doe, R. Thorpe, B. Paulsson, J.E. Gale, and C. Forster. (LBL-8570, SAC-18).

19. Fracture Detection in Crystalline Rock Using Ultrasonic Shear Waves by K.H. Waters, S.P. Palmer, and W.F. Farrell. (LBL-7051, SAC-19).

20. Characterization of Discontinuities in the Stripa Granite--Time Scale Heater Experiment by R. Thorpe. (LBL-7083, SAC-20).

21. Geology and Fracture System at Stripa by A. Okliewicz, J.E. Gale, R. Thorpe, and B. Paulsson. (LBL-8907, SAC-21).

22. Calculated Thermally Induced Displacements and Stresses for Heater Experiements at Stripa by T. Chan and N.G.W. Cook. (LBL-7061, SAC-22).

23. Validity of Cubic Law for Fluid Flow in a Deformable Rock Fracture by P.A. Witherspoon, J. Wang, K. Iwai, and J.E. Gale. (LBL-9557, SAC-23).

24. Determination of In-Situ Thermal Properties of Stripa Granite from Temperature Measurements in the Full-Scale Heater Experiments: Methods and Primary Results by J. Jeffry, T. Chan, N.G.W. Cook and P.A. Witherspoon. (LBL-8424, SAC-24).

25. Instrumentation Evaluation, Calibration, and Installation for Heater Tests Simulating Nuclear Waste in Crystalline Rock, Sweden by T. Schrauf, H. Pratt, E. Simonson, W. Hustrulid, P. Nelson, A. DuBois, E. Binnall, and R. Haught. (LBL-8313, SAC-25)

26. Part I: Some Results From a Field Investigation of Thermo-Mechanical Loading of a Rock Mass When Heater Canisters are Emplaced in the Rock by M. Hood. Part II: The Application of Field Data from Heater Experiments Conducted at Stripa, Sweden for Repository Design by M. Hood, H. Carlsson, and P.H. Nelson. (LBL-9392, SAC-26).

27. Progress with Field Investigations at Stripa by P.A. Witherspoon, N.G.W. Cook, and J.E. Gale (LBL-10559, SAC-27).

28. A Laboratory Assessment of the Use of Borehole Pressure Transients to Measure the Permeability of Fractured Rock Masses by C.B. Forster and J.E. Gale. (LBL-8674, SAC-28).

29. Thermal and Thermomechanical Data for In Situ Heater Experiments at Stripa, Sweden by T. Chan, E. Binnall, P. Nelson, O. Wan, C. Weaver, K. Ang, J. Braley, and M. McEvoy. (LBL-11477, SAC-29).

30. The Effect of Radon Transport in Groundwater Upon Gamma Ray Borehole Logs by P.H. Nelson, R. Rachiele, and A. Smith. (LBL-11180, SAC-30).

31. Strength and Permeability Tests on Ultra-Large Stripa Granite Core by R. Thorpe, D.J. Watkins, W.E. Ralph, R. Hsu, and S. Flexser. (LBL-11203, SAC-31).

32. Ultrasonic and Acoustic Emission Results from the Stripa Heater Experiments. Part I: A Cross-Hole Investigation of a Rock Mass Subjected to Heating by B.N.P. Paulsson and M.S. King. Part II: Acoustic Emission Monitoring During Cool-Down of the Stripa Heater Experiment by R. Rachiele. (LBL-10975, SAC-32).

33. Numerical Modeling to Assess Possible Influence of the Mine Openings on Far-Field In Situ Stress Measurements at Stripa by T. Chan, V. Guvanasen, and N. Littlestone (LBL-12469, SAC-33).

34. A Field Assessment of the Use of Borehole Pressure Transients to Measure the Permeability of Fractured Rock Masses by C.B. Forster and J.E. Gale. (LBL-11829, SAC-34).

35. Water Inflow into Boreholes During the Stripa Experiments by P.H. Nelson, R. Rachiele, J.S. Remer and H.S. Carlsson (LBL-12547, SAC-35).

TABLE OF CONTENTS

LIST OF FIGURES

LIST OF TABLES

ABSTRACT

To better define the character of the rock encompassing the thermo-mechanical and hydrological experiments at the Stripa mine in central Sweden, and to help determine the size of the Stripa pluton, detailed studies were conducted of the petrology and radiogeology of the quartz monzonite and adjacent rocks. Petrologic studies emphasized optical petrography, with supplementary X-ray diffraction, X-ray fluorescence and microprobe analyses. Radiogeologic investigations were based primarily on surface and under-ground gamma-ray spectrometric measurements of uranium, thorium and potassium, supplemented by laboratory gamma spectrometric analyses and fission-track radiographic determinations of the locations and abundance of uranium in the rock matrix.

Both the quartz monzonite and the metavolcanic leptite which it intruded are strongly fractured. Two stages of fracture filling are evident; an earlier stage encompassing quartz, sericite, feldspar, epidote, and chlorite, and a later stage dominated by carbonate minerals.

The Stripa quartz monzonite is chemically and mineralogically distinct from other plutons in the region. Muscovite is the predominant mica in the quartz monzonite; biotite has been altered to chlorite, hornblende is absent, and accessory minerals are scarce. In contrast, in other plutons in the Stripa region biotite and hornblende are prominent mafic minerals and accessory minerals are abundant.

The Stripa quartz monzonite is also considerably more radioactive than the leptite and other plutons in the region. Uranium and thorium abundances are both ~ 30 ppm, considerably higher than in "normal" granitic rocks where the thorium-to-uranium ratio generally exceeds 2.

Potassium-argon dating of muscovite from the Stripa quartz monzonite indicates that this rock may be older, at 1691 million years than granitic rock of the neighboring Gusselby and Kloten massifs, whose ages, based on K-Ar dating of biotite, are respectively 1604 and 1640 m.y.

Heat flow and heat productivity considerations show that although Stripa quartz monzonite contains high abundances of radioelements, the pluton has little effect on the regional heat flow. If it occurs in a layered plutonic setting, it is not more than 1.5 km thick; otherwise it may comprise a stock, dike, or border phase that is relatively small compared with the large granitic plutons exposed in the region.

1.0 INTRODUCTION

A number of geomechanical, hydrological, and geochemical tests have
been conducted over the past three years in granitic rock at the Stripa
mine in central Sweden. More than 30 reports describing the Swedish-American
cooperative program have focused on the hydrologic setting and the response
of the rock to heating. The results of these tests will be used to establish
techniques for measuring the hydrological, geomechanical and geochemical
settings of proposed nuclear waste repositories and to determine the properties
of a granitic rock mass that would be critical for the long-term isolation of
radioactive waste.

To validate the transferability of these techniques and properties
from Stripa to the evaluation of potential repository masses, it is necessary
to know, in some detail, the geologic setting and petrology of the Stripa
pluton. The general geologic setting was the subject of a report by the
Geological Survey of Sweden (Olkiewicz et al., 1978), and the fracture system
and lithology of the underground workings were described more recently by
Olkiewicz et al. (1979). The experiments at Stripa are being conducted in a
body of quartz monzonite* within ~ 200 m of its contact with older meta-
morphic rock. Yet, little is known of the size and configuration of the
Stripa pluton. On the recently published geologic map of the Lindesberg
Southwest quadrangle (Koark and Lundström, 1979), the pluton is shown exposed
over a relatively small area (~ 0.3 km radius). However, the extensive cover
of glacial debris, as shown on the soils map of the region (Geological Survey
of Sweden, 1977), may obscure the true size and shape of the pluton at the

---

*This usage of the term "quartz monzonite" follows common American nomen-
clature of igneous rocks. According to classification of the IUGS (1973),
however, this rock would be termed "granite."

surface. The configuration of the contact with depth between the pluton and
the metamorphic rock (leptite) is well defined only to the south, afforded by
the workings of the old iron mine (Olkiewicz et al., 1978, 1979). Contacts
to the north, west, and east are concealed at the surface and unexplored
at depth. Thus, it is unknown whether the granitic rock mass at Stripa
is, among other things, a dike-like body, a stock, or the exposed portion of
a much larger pluton, and therefore the position of the experiments within
the pluton also remains in question.

To help answer these questions, a program of geological studies was started
in the summer of 1979 to determine the size, configuration and composition of
the Stripa pluton. Samples of granitic and metamorphic rocks were collected
from the surface and underground at Stripa and at other plutons within the
Lindesberg region.* (The regional sample locations are shown in Fig. 1, those
closer to the Stripa mine in Fig. 2, and underground in Figs. 3 and 4). Samples
of cores were also selected from the inclined holes SBH 1 and 2, drilled from
the surface toward the experimental area, and from the vertical hole DBH V-1,
drilled to a length of ~ 470 m from the mine's 410 m level; holes SBH-2 and
DBH V-1 are shown in cross section, Fig. 5. This set of samples then covers
a vertical extent from the surface to a depth of nearly 900 m and encompasses
predominantly quartz monzonite and leptite as well as pegmatite, diabase, and
amphibolite. The sample set also contains representatives of the classes of
fractures encountered in the Stripa pluton: those filled predominantly by
chlorite, those by epidote and sericite, and those by quartz and carbonate

---

*A large number of the samples from other plutons and their major oxide
analyses were kindly provided by I. Lundström of the Geological Survey
of Sweden (SGU). The description of these samples is included as Appendix C.

YOUNGER GRANITIC ROCKS

OLDEST GRANITIC ROCKS

METAVOLCANIC ROCKS, INCLUDING LEPTITES

GABBRO AND DIORITE

LIMESTONE AND MARBLE

METASEDIMENTARY ROCKS

DIABASE

SWEDEN
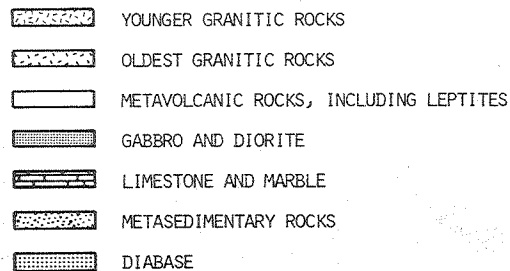
Stripa

MAP NUMBER	SAMPLE NUMBER
1	IL 79-1
2	I 75-10
3	I 75-11
4	I 75-22
5	C 75-9
6	C 75-10
7	C 75-11
8	ST-48
9	ST-47
10	ST-46
11	J 75-9
12	J 75-8
13	J 75-4
14	J 75-7

KLOTEN

KOPPARBERG

DAMMSJÖN

STRIPA

GUSSELBY

LINDESBERG

FELLINGSBRO

N

20 km

-3-
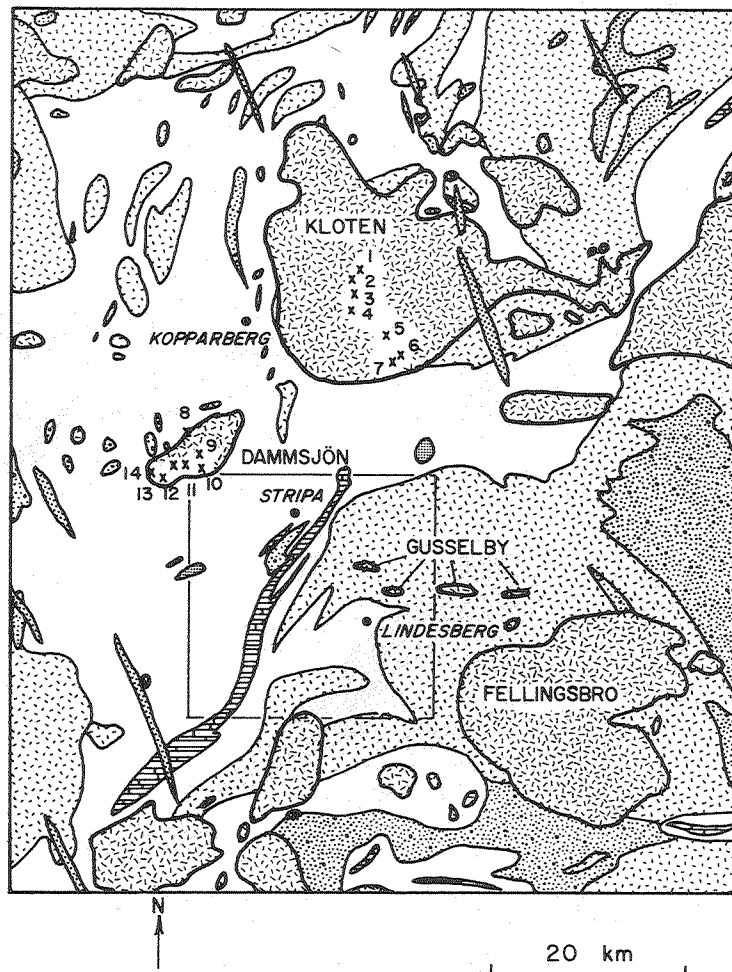
XBL 814-9185

Fig. 1(a). Simplified geologic map of the Stripa region showing sample locations. Area
within the square in the map is enlarged and shown as Fig. 1(b). Geologic
base map from the Bedrock Map of Sweden, published by the Swedish Geological
Survey, 1958, and the Geological Map of Lindesberg SW Quadrangle, also
published by S.G.U., 1979.
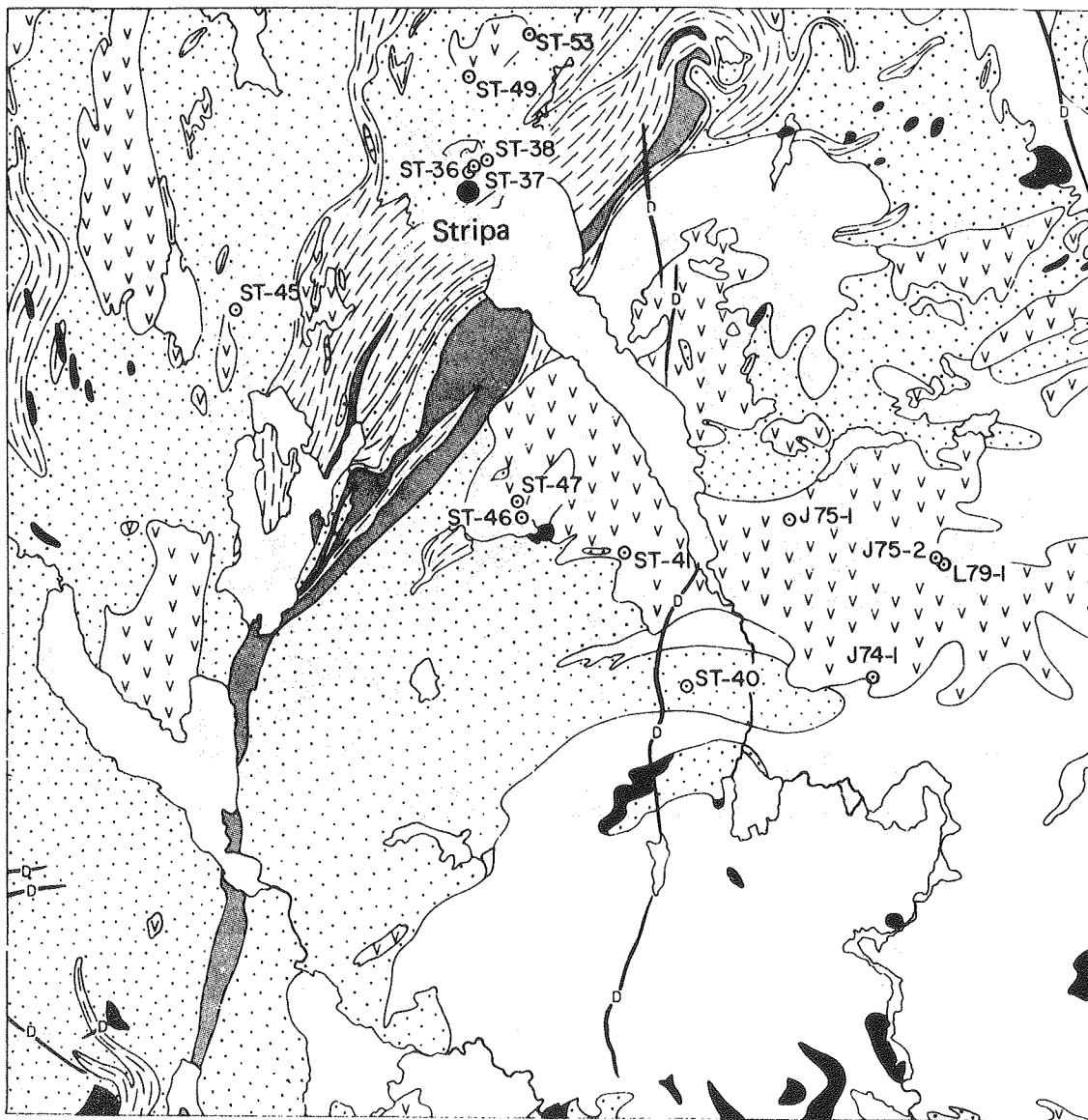
Fig. 1(b). More detailed geologic map of the Stripa area showing sample and field gamma measurement locations. Geologic base from Olkiewicz et al., 1978.
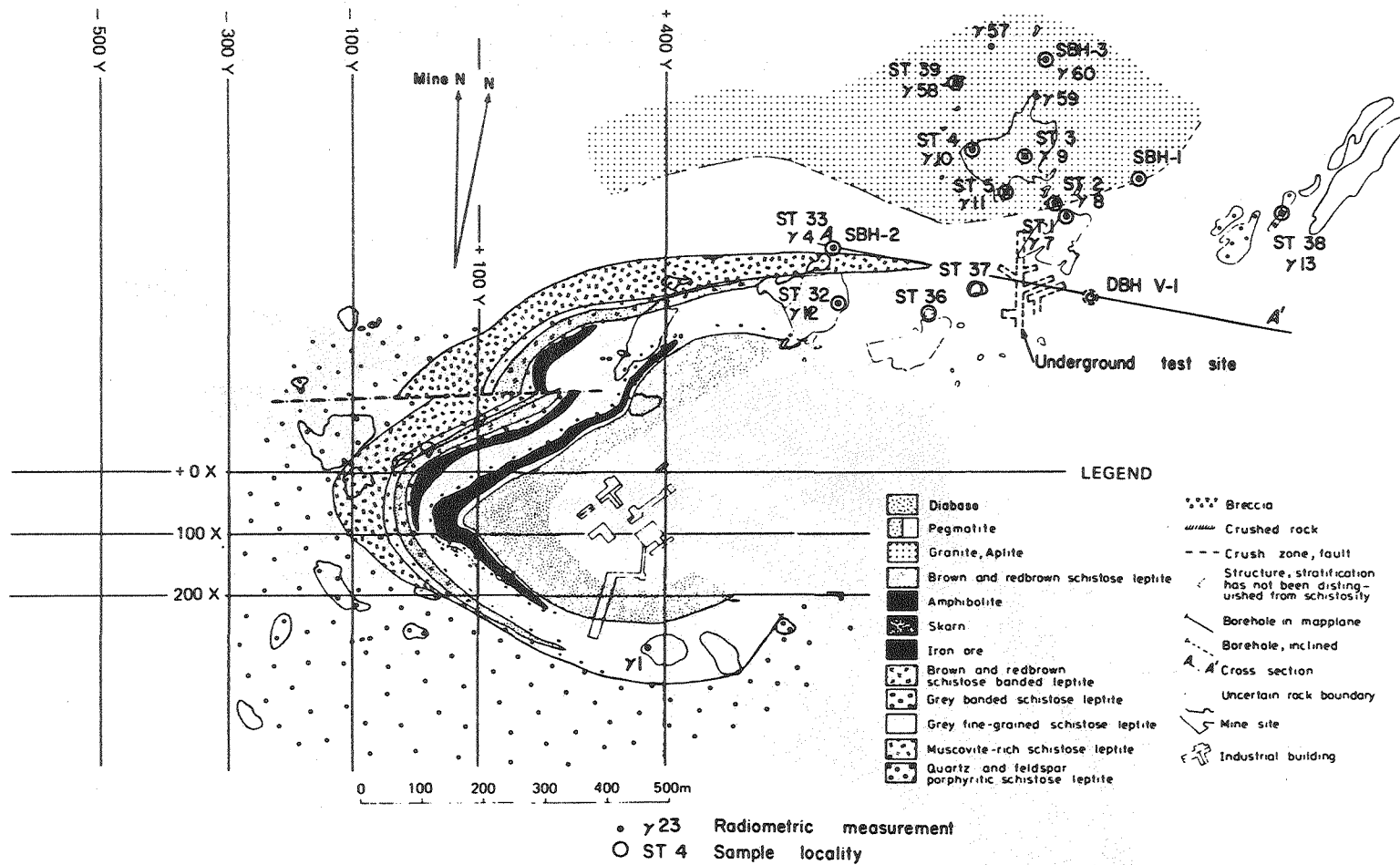
Fig. 2. Geologic map of the Stripa mine area showing sample and field gamma measurement locations. Geologic base from Olkiewicz et al., 1978.
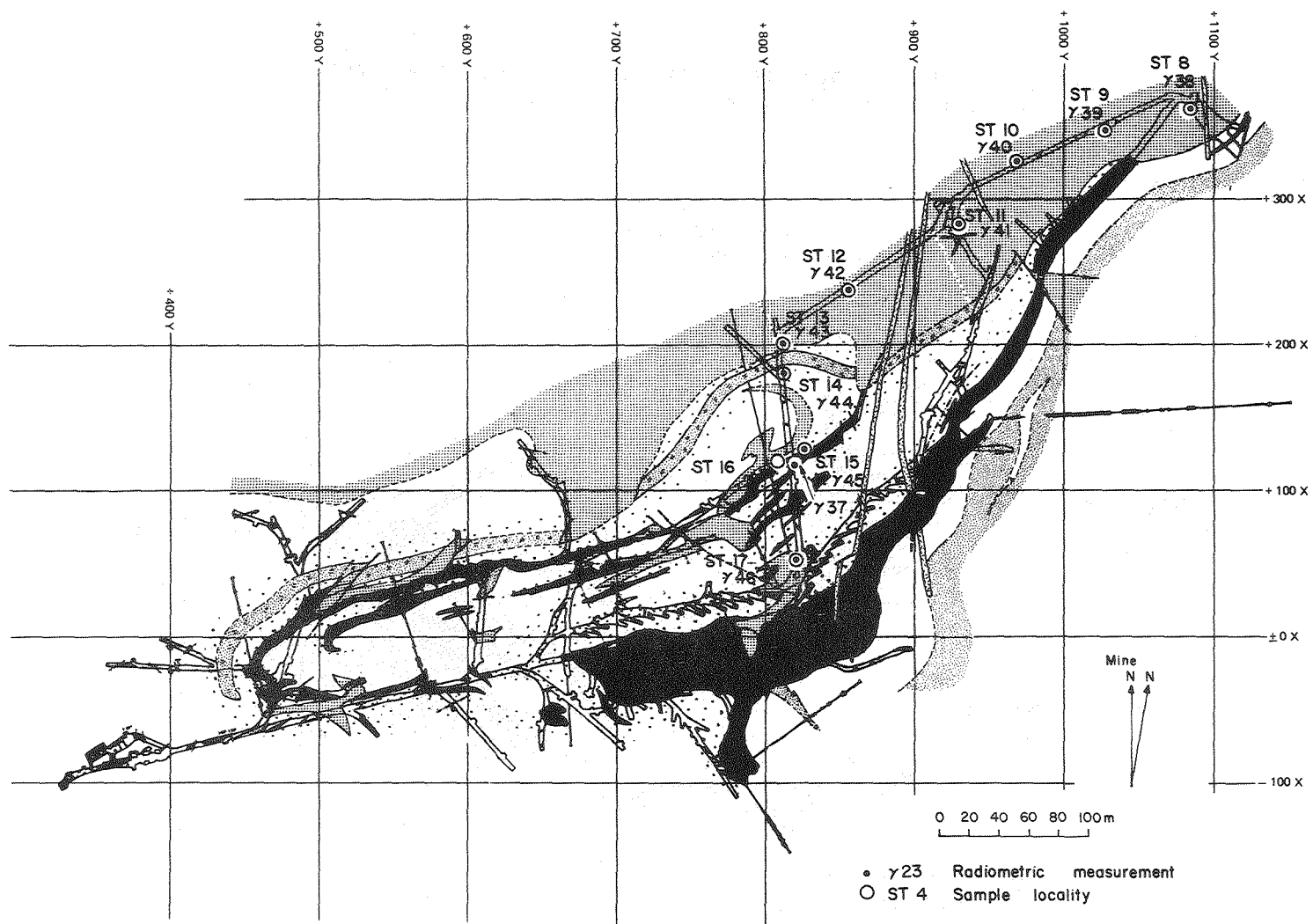
XBL 8010-7372A

Fig. 3. Geologic map of the 310 m level of the Stripa Mine showing sample
and gamma measurement locations. Geologic base from Olkiewicz et al.,
1978. Legend is the same as in Fig. 2.

XBL 8010-7371
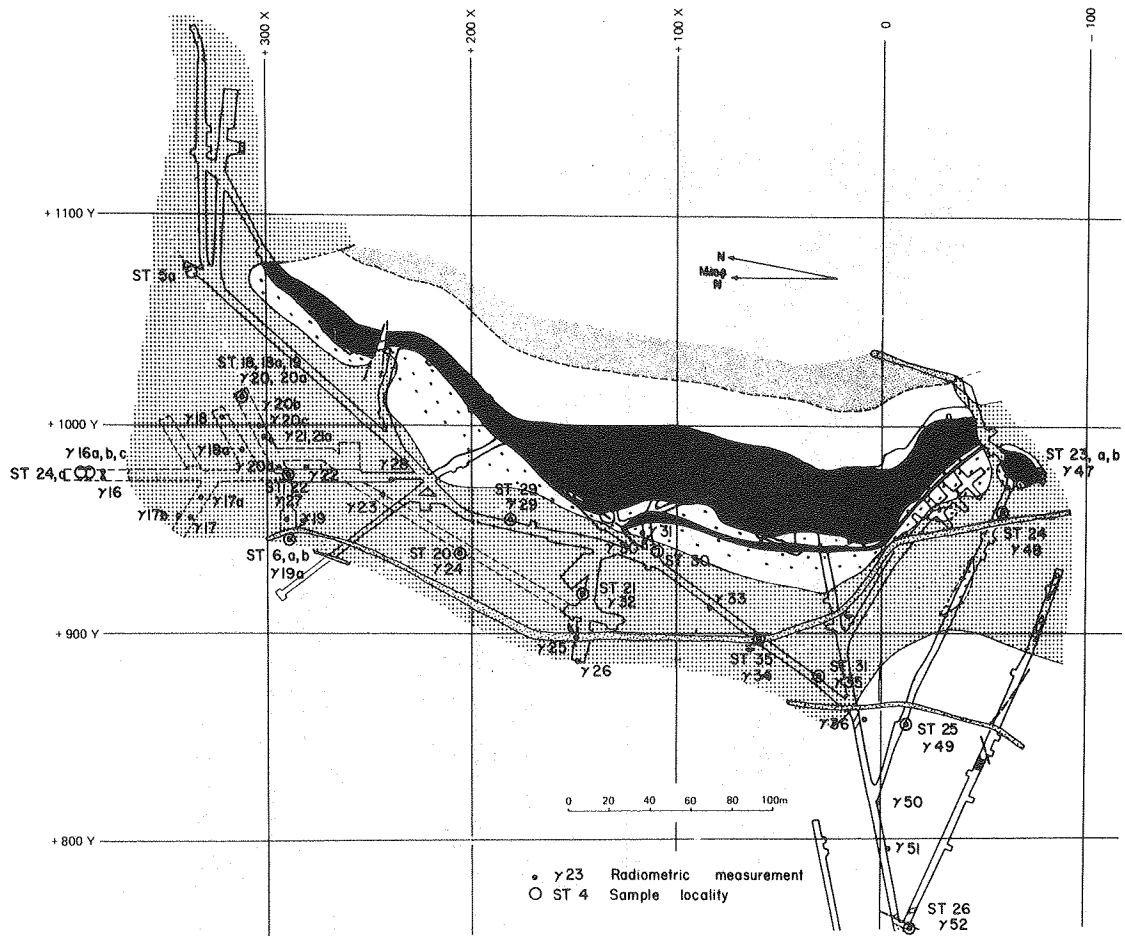
XBL 8010-7369

Fig. 4(a). Geologic map of the 360 m level of the Stripa mine showing sample and gamma measurement locations. Geologic base from Olkiewicz et al., 1978. Legend is the same as in Fig. 2.
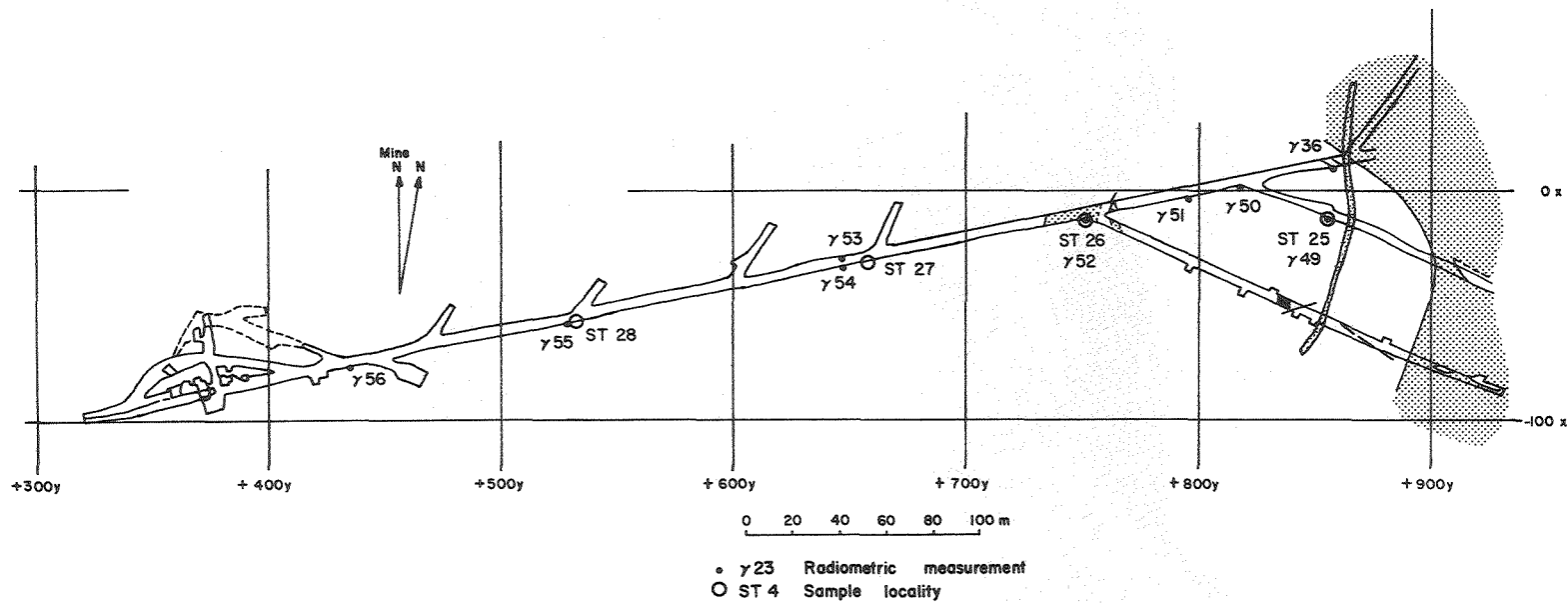
Fig. 4(b). Westward continuation of Fig. 4(a), with the appropriate
coordinates. The axis of the figure is rotated 90°.
Note: The area of overlap of Figs. 4(a) and 4(b) includes sample
sites ST-25 and ST-26. Legend is the same as in Fig. 2.
Geologic base from Olkiewicz et al., 1978.
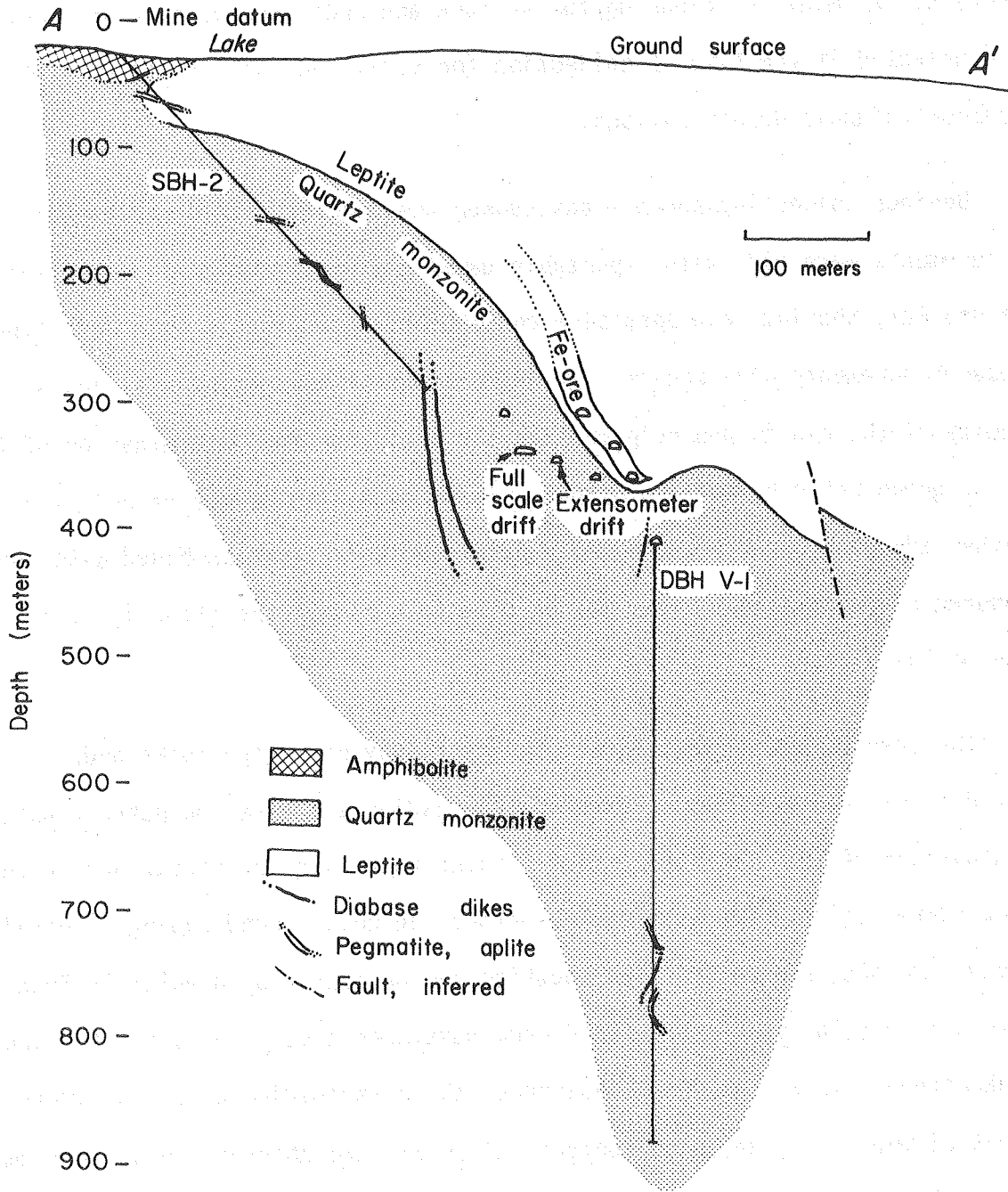
Fig. 5. Vertical cross-section bearing N89°E through boreholes SBH-2 and DBH V-1.

minerals. At many locations on the surface and underground, hand specimens were oriented at the time of collection for strike and dip, to permit subsequent petrofabric determinations.

Besides collecting surface and subsurface samples, field radiometric measurements were made with a portable gamma-ray spectrometer to determine the uranium, thorium, and potassium concentrations of the various rock types. These measurements give preliminary indications of the geochemical homogeneity of the pluton and help provide the basis for the determination of the age of groundwater by the ^{4}He method. These data also permit calculation of the radiogenic heat production, a parameter that, when combined with the measured conductive heat flow, may be used to estimate the effective thickness of the pluton.

This report emphasizes, first, the petrology of Stripa rocks and, second, their radiogeology. Petrological results are based on petrographic examinations of thin sections of the various rock types at Stripa and in the surrounding region. The results of surface and underground radiogeological surveys are also presented. The location and abundance of uranium in fractures and in relatively unfractured rock have been discerned by the fission-track method. This provides a measure of the distribution of the ultimate parent element of ^{222}Rn, high contents of which were observed in water from drill holes in the experimental area (Nelson et al., 1980).

2.0 PETROLOGY

2.1 Techniques

Petrographic interpretation of thin sections was a major focus of this portion of the study, and descriptions of individual thin sections have been compiled in Appendix A. This work has been supplemented by X-ray diffraction and microprobe analyses, and by X-ray fluorescence chemical analyses of several of the granitic rocks. Also, fission-track radiography was used to determine the location and abundance of uranium in several samples.

2.2 Matrix Mineralogy of Stripa Quartz Monzonite

Stripa quartz monzonite is predominantly a grey or reddish, medium to fine-grained, relatively uraniferous granitic rock of Proterozoic age. It shows abundant fracturing and deformation on a microscopic scale and frequently on a macroscopic scale as well. On the basis of both chemical composition (see Section 2.6) and relative abundance of its primary minerals, it is more accurately classified as a quartz monzonite than a "granite" (see footnote, p.1).

The granitic matrix--a term designating the primary minerals that crystallized from the melt, as opposed to secondary alteration minerals or fracture-filling minerals--is composed mainly of quartz, plagioclase, and microcline, with lesser muscovite and biotite (now altered to chlorite), and accessory opaque minerals, garnet, and zircon.

Table 1 shows the mineral composition of Stripa quartz monzonite samples, all but one relatively unfractured, along with compositions of neighboring plutons. These results are also plotted in Fig. 6, illustrating the relative abundances of quartz, plagioclase, and microcline.

Table 1. Mineral composition (modal analyses based on point counts) of granitic rocks from Stripa and neighboring plutons. Stripa samples are of relatively unfractured quartz monzonite, with the exception of E 13b.

	Stripa						Gusselby			Kloten			Dammsjön	
	S-12	S-38	E7-2	E14b	E29b	E13b	J75-1	J74-1	L79-1	C75-11	C75-9	I75-10	J75-14	J75-9
Qtz	37.1	35.3	35.8	28.7	34.1	41.1	38.2	33.8	29.1	40.4	44.3	32.6	34.5	31.6
Plag	32.0	35.1	27.6	32.8	26.7	25.9	24.8	19.0	31.1	24.3	25.3	25.0	30.0	38.9
K-fsp	22.2	21.5	25.4	34.4	32.9	18.0	28.2	43.7	36.1	20.7	26.2	41.8	31.0	17.3
Musc/ Seric	7.4	4.0	6.4	3.2	3.9	}12.5	1.2	1.5	0.5	-	-	-	1.7	-
Chlor	1.3	4.1	4.5	2.8	2.4		}7.5	}1.6	}3.2	<1	<1	}0.6	<1	1.9
Biot	-	-	-	-	-	-				12.6	4.2		-	7.2
Amph	-	-	-	-	-	-	-	-	-	<0.5	-	-	-	1.7
Sphene	-	-	-	-	-	-	-	-	-	1.5	-	-	-	0.8
Access[a]	<1	<1	<1	<1	<1	2.4	<1	<1	<1	<1	<1	<1	2.6	<1
	(O,C,Z)	(E,F,G)	(F,O,G)	(C)	(C,O,F)	(C,O)	(Z,F,C,O)	(O,Z,A)	(Z,E,C,O)	(A,Z,F)	(O,Z)	(O)	(O,E)	(O,E,A)

[a] Accessory minerals: O - opaques; C - carbonate; E - epidote; F - fluorite; Z - zircon; G - garnet; A - apatite

Samples with E prefix are from the extensometer holes drilled in the full-scale and extensometer drifts. See Appendix A for locations and descriptions of other samples.

-12-

MODES

STRIPA   PLUTON
① S-12
② S-38
③ E7-2
④ E-13b
⑤ E-14b
⑥ E-29b

GUSSELBY   MASSIF
① J74:1
② J75:1
③ L79:1

KLOTEN   MASSIF
1 C75-9
3 C75-11
4 I 75-10

DAMMSJÖN   MASSIF
▲ J:75:9
▲ J:75:14
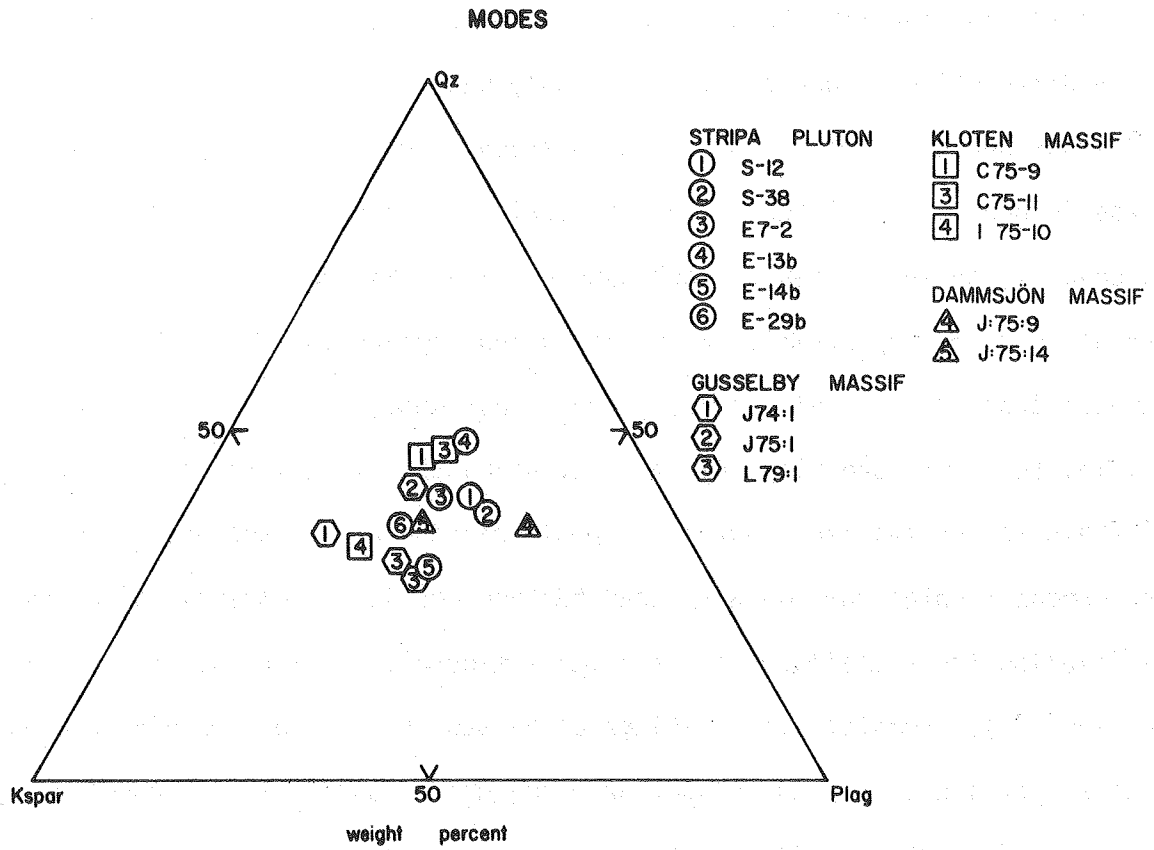
XBL 814-9189

Fig. 6.   Relative model abundances of quartz, microcline, and
plagioclase, normalized to 100% of Stripa and neighboring
granites.

Oligoclase is the probable species of plagioclase present in the quartz monzonite, judging from occurrences in chemically similar granites, and from X-ray diffraction evidence. It invariably has a dusty appearance in thin sections, due to growth of minute alteration products. In addition, plagioclase is generally altered in part to sericite (fine-grained, secondary muscovite), or less often to carbonate or clay. Microcline is commonly perthitic or microperthitic, with alteration similar to, but much less intense than, that in plagioclase, and is not dusty. Microcline is often interstitial to quartz and plagioclase, suggesting that it was the last of these minerals to crystallize. Quartz is unaltered and clear, and quartz grains are commonly intergrown in a sutured texture possibly indicative of recrystallization (recrystallization of primary minerals is discussed further in Section 2.4). Hematite is sometimes dispersed as fine dust within feldspar grains, particularly plagioclase, or along grain boundaries or cracks within grains, and is responsible for the red color of many granitic samples.

Muscovite occurs clear and unaltered, as well as partially altered to chlorite and sericite. Replacement generally advances along cleavage planes. Biotite, at one time a constituent of the matrix, is now thoroughly altered to dark green chlorite, with occasional brown biotite remnants in chlorite providing the only direct evidence for this replacement. However, chlorite is not known to crystallize as a primary mineral (Deer et al., 1962); it is a common pseudomorphous hydrothermal alteration product of biotite in granitic rocks where its chemical composition is generally related to that of the original biotite. Table 2 lists a partial chemical analysis

Table 2. Electron microprobe analysis of chlorite grains from sample of Stripa quartz monzonite from 4.60 m depth in borehole N1 in time-scaled drift. Data averaged over 30 points.

Oxide	Weight %	Std. Deviation
Fe_2O_3[a]	38.04	1.02
MgO	6.25	0.33
SiO_2	24.99	0.95
Al_2O_3	19.09	0.65

[a] Total iron expressed as Fe_2O_3. Oxidation state of iron unknown.

The abundance of the four major elements in chlorite were obtained on the electron microprobe of the Department of Geology and Geophysics at the University of California at Berkeley. Other elements analyzed were Na, Ca, Zr, and U; their oxides were generally present only in trace amounts (<0.1 wt. %). Thus, the total percentage by weight of analyzed oxides was ~ 88.4%; this, with the 10-13% H_2O by weight commonly reported in chlorites, brings the total to close to 100%.

by electron microprobe of chloritized biotite in one sample of quartz
monzonite from the time-scaled drift. This chlorite analysis is compar-
able to analyses of biotites in granites, particularly with respect to
values of Fe_2O_3 and MgO (Deer et al. 1962), and is thus consistent
with an origin of the chlorite by replacement of primary biotite.

Garnet, possibly spessartine-almandine (Mn-Fe), is a common accessory
mineral in the Stripa quartz monzonite. It occurs generally as isolated
unaltered anhedral grains up to 0.5 to 1.0 mm in diameter; these grains are
often anisotropic. In certain aplitic samples, however, garnet grains are
much more abundant (see description of S-39 in Appendix A), and are often
rounded and partially altered to chlorite. Very fine grains of accessory
minerals, both opaque and non-opaque, are common in the chloritized biotite
of the matrix. Pleochroic halos, indicating the presence of elements of the
U or Th decay series, are often strongly marked in the chlorite surrounding
these grains. The opaque grains have not been identified, but the others are
probably zircon. Their optical properties do not definitely identify them as
zircon, but several grains analyzed by microprobe in the chlorites of
Table 2 have high contents of zirconium.

2.3 Fracture Fillings in Stripa Quartz Monzonite

The Stripa quartz monzonite is characterized by a great abundance
of fractures and a variety of fracture-filling minerals. Fractures ranging
from well under a millimeter to several centimeters or more in width, as well
as wider zones of brecciation, are readily visible in hand sample; but only
in thin section does the full extent of fracturing and brecciation become
apparent. The great majority of fractures have been completely sealed, but

in some cases fine openings can be seen in thin section. It is not certain which of these smaller openings may have formed in response to unloading of stresses during core removal, and which existed in the rock prior to drilling.

2.3.1 Descriptions of Materials

In hand sample, fracture fillings often can be easily classified on the basis of color, with dark green to black, light green, and white fractures most common. In thin section, however, such a simple classification scheme is not possible because the fractures are filled with intergrown minerals in different combinations, combinations that often have similar colors in hand sample.

The most common fracture-filling minerals are chlorite, sericite, quartz, epidote, and carbonate minerals, with fluorite and opaque minerals (often pyrite or hematite) somewhat less common. The thickness of fractures spans a wide range, from less than 0.01 mm (10 μm) to centimeters. (The terms "stringers," "fine fractures," or "fine veins" will be used often to refer to fractures less than 0.05 mm wide.) Generally, only finer fractures are filled with single minerals, usually quartz, sericite, chlorite, or carbonate. Coarser fractures almost invariably are filled with intergrowths of two or more minerals, most often sericite and chlorite. Quartz occurs in combination with any of the fracture-filling minerals. Epidote is usually associated with quartz, chlorite, or sericite, as is carbonate, which is sometimes intergrown with fluorite as well. Fluorite is usually intergrown with quartz, carbonate, chlorite, or, rarely, epidote. Pyrite is sometimes intergrown with sericite and chlorite.

In megascopic appearance, the following generalizations are useful, though not foolproof: dark green or black fractures are usually dominated by chlorite; white or near-white fractures by quartz and/or carbonate. Light green fractures are more ambiguous, as they may be a mixture of the above types, or they may be filled mainly with sericite (fine fractures particularly), or with epidote, or, in wide brecciated zones, with a clay-rich fault gouge.

On the finest scale, stringers of sericite and chlorite, quartz and, less commonly, feldspars are abundant, but are not visible megascopically (Fig. 7). They are generally discontinuous and of limited extent, and fill cracks in primary grains or along grain boundaries. These stringers are common in both fractured and relatively unfractured quartz monzonite, and probably relate either to an early deformation or to a late stage in the cooling history of this rock.

Another, more unusual fracture-filling material has been found, although rarely, in the Stripa quartz monzonite. This material is a hydrocarbon mineral, asphaltite, and is closely associated with calcite and scattered opaque grains in fractures in borehole SBH-4, drilled from the surface in summer 1980. The asphaltite is a high-weight variety, a high-temperature distillate that is dark brown to black, hard, and highly aromatic (B. Simoneit, University of California, Los Angeles, Institute of Geophysics and Planetary Physics, personal communication). It is ~ 1 cm wide at its most prominent occurrence in borehole SBH-4, but in general it has been found in fractures ranging in width

0.25 mm
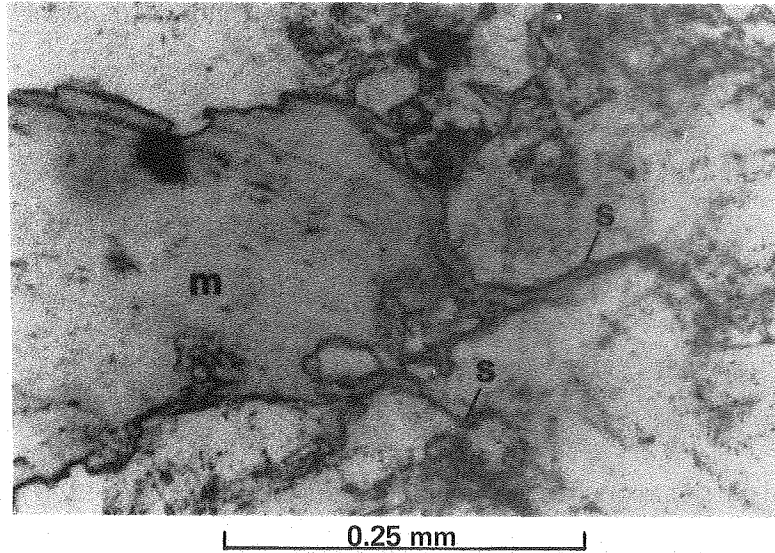
Fig. 7.   (A) Fine sericite-filled cracks (s) extending from
primary muscovite grain (m) in quartz monzonite,
S-38. Cracks intersect grains of quartz and feldspar.
Plane-polarized light.

0.25 mm   XBB 800-13603A
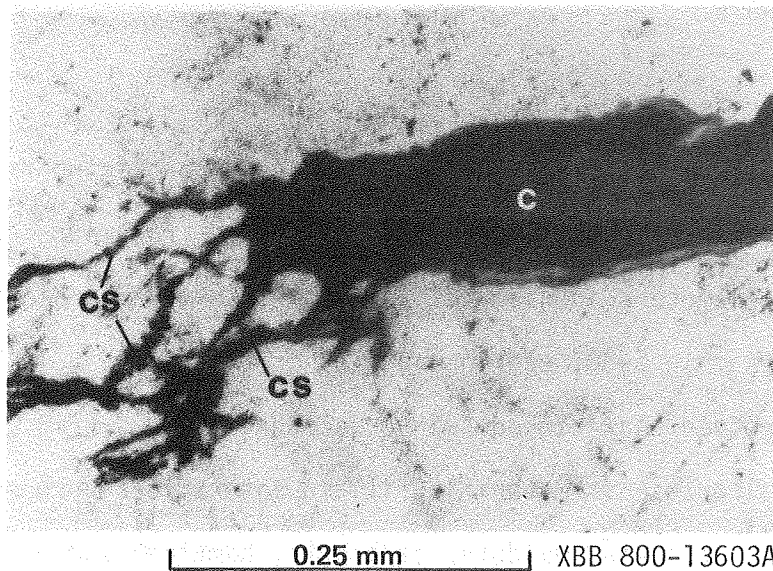
(B) Chlorite analogue of (A). Chlorite stringers (cs)
associated with grain of biotite completely altered
to chlorite (c) in quartz monzonite, S-26. Plane-
polarized light.

from 1 mm to < 0.1 mm. Adjacent to these fractures, asphaltite can also be found in very fine interstices between quartz and feldspar grains, and even in cleavage planes in muscovite.

The origin of the hydrocarbon is a puzzle, as is the time at which it was deposited in the quartz monzonite. One hypothesis is that its ultimate source was the organic matter in limestones and dolomites, some of which, now metamorphosed to marble, are exposed within several kilometers of Stripa (Fig. 1b). This organic-derived hydrocarbon could have been mobilized in carbonate-rich fluids during metamorphosis, and redeposited in distilled form, along with calcite, in fractures in the quartz monzonite.

Opaque grains associated with these asphaltite-filled fractures often contain significant concentrations of uranium, and these are discussed further in Section 3.5.

2.3.2 Breccias

In wide fractures or fracture zones, breccias containing fragments of the granitic parent rock are usually a major component. Fragments are generally up to several millimeters in diameter (sometimes to several centimeters) and may be angular (sample S-30, see Appendix A) or rounded (S-23) (Fig. 8); included crystals often show kinked twin or cleavage planes (Fig. 9) and a high degree of alteration. Materials filling interstices between fragments include chlorite, sericite, epidote, carbonate, hematite and other opaques, fluorite, clay, and finely comminuted quartz and feldspar grains.

In some prominent wide fractures, breccia is not the dominant filling material, but instead is either absent or present only as lenses surrounded
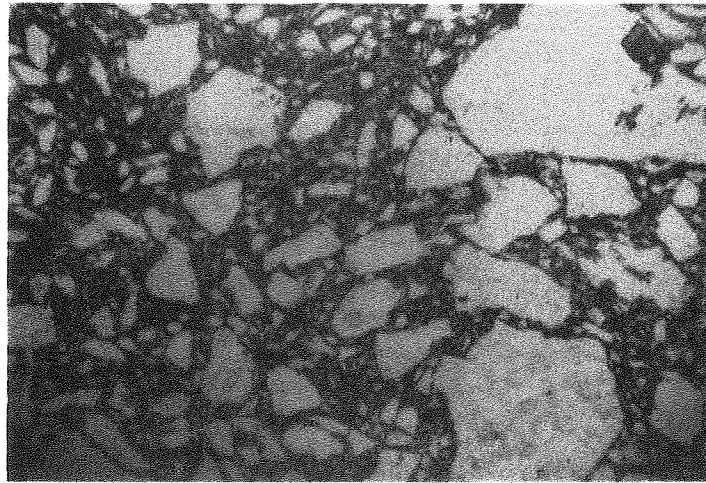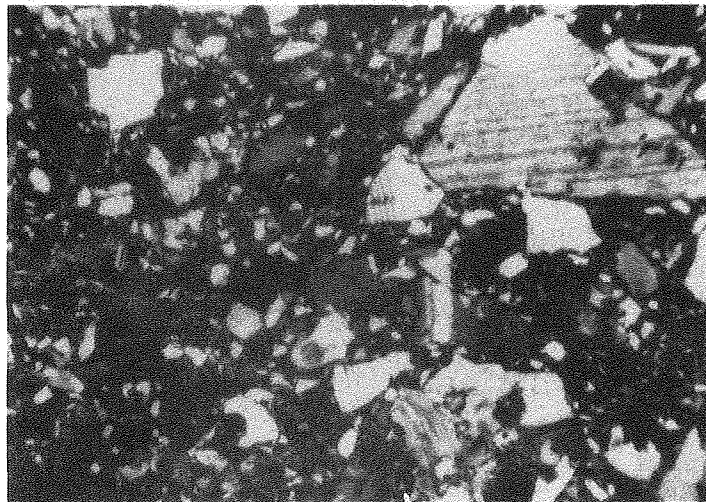
0.5 mm

0.5 mm   XBB 800-13610A

Fig. 8.   Granitic breccia, S-46, composed of grains of
          quartz, plagioclase, microcline, and composites
          of these minerals, fragmented from the parent
          quartz monzonite. Coarser fragments are generally
          angular, and finer fragments more rounded. Inter-
          stitial material is very finely granulated quartz
          and feldspar, with intergrown chlorite. (A) plane-
          polarized light; (B) cross-polarized light.
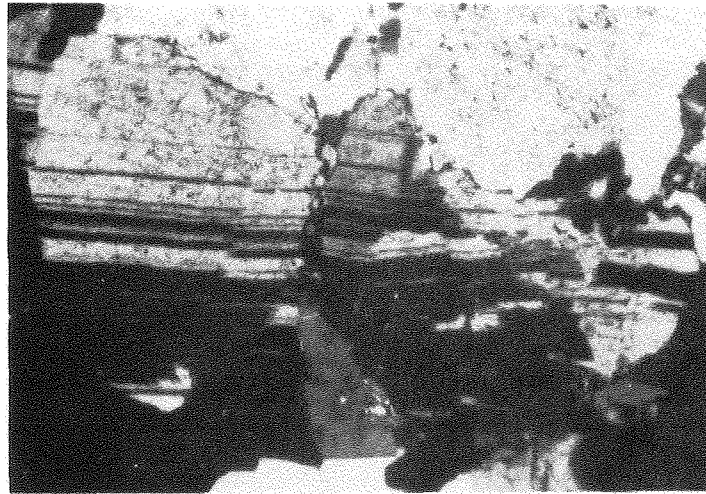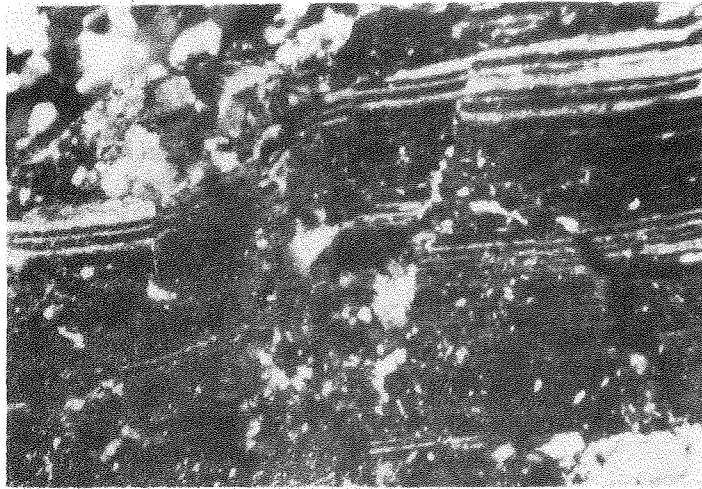
Fig. 9. Displaced twin lamellae in plagioclase grains, in fractured and brecciated quartz monzonite. Lamellae are displaced along cracks in (A) (S-29), while in (B) (S-33), lamellae are bent as well as fractured. Grain in (B) is partly altered to sericite. Cross-polarized light.

by fracture-filling minerals. Such fractures are generally dominated by carbonate (e.g., S-47) or, more frequently, by chlorite. Chlorite occurs alone or in a densely intergrown mosaic with quartz or sericite. Lenses rich in epidote or opaque materials are sometimes present (S-43, S-47), and pyrite may be locally abundant (S-28). Often, wide fractures are foliated due to alignment of lenses of various materials. Foliation is also accentuated by parallel orientation of fine veins within the fracture zones (Fig. 10). Where breccia is a component of the fracture-filling, it sometimes develops the texture of mylonite gneiss (S-33, S-42).

In addition to the coarse breccias common in wide fracture zones,fine-grained breccias, visible only in thin section, are abundant in the quartz monzonite. These have been termed "microbreccia" and consist of a tight mosaic of broken angular quartz and feldspar grains, with very sparse, generally chloritic interstitial fillings. They often form where two or more fractures converge to become one wider fracture, or where fine fractures become so pervasive that the matrix is no longer distinguishable. Microbreccia also occurs in discrete veins and in lenses in wider fractures.

2.3.3 Fracture Sequences

The sequence of formation of the various types of fractures is generally uncertain on the basis of petrographic interpretation alone. However, for the fine, discontinuous stringers of quartz, feldspar, sericite, or chlorite discussed above, the evidence suggests that these fractures belong to an early stage of deformation. Also, fractures dominated by carbonate sometimes cut across and offset fractures filled with other materials (a relationship seen also in leptites) and carbonate also occurs as a last in-filling of coarse
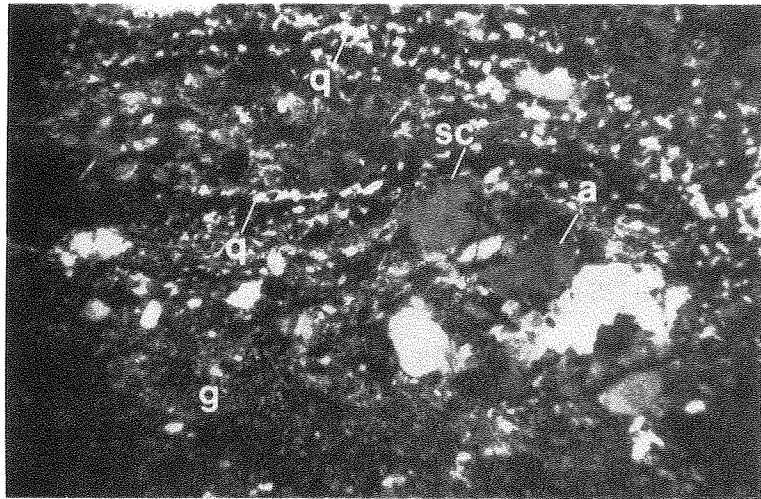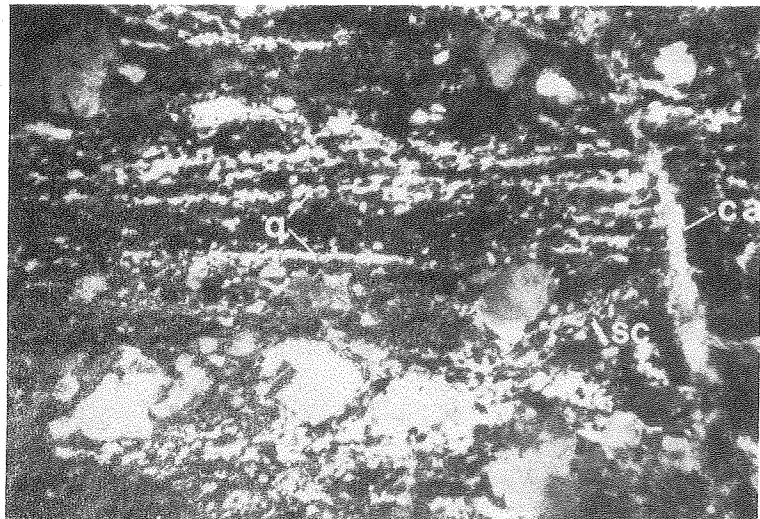
0.5 mm

0.5 mm   XBB 800-13606A

Fig. 10. Mylonitic breccia in contact zone between quartz
          monzonite and dike, S-33. Strong foliation is
          defined by layers of fine recrystallized quartz (q),
          and by stringers of sericite and chlorite (sc)
          running through the breccia or bordering fragments of
          parent granitic rock. Foliation is convoluted in (A)
          adjacent to the granitic augen (a), and is parallel in
          (B). Very finely granulated granitic rock occurs in
          dense aggregates (g) and in interstices between larger
          fragments. Fracture filled with carbonate mineral
          (ca) cuts across foliation in (B). Cross-polarized
          light.

fractures. Thus it is likely that carbonate desposition belongs to the latest stage of fracturing. Fractures filled with other materials do not show a similar consistent pattern, and their formation may have spanned a wide period in the fracture history of the quartz monzonite.

2.3.4. Open Fractures

Open fractures, although not abundant, have been observed in some samples. They are generally about 0.05 mm wide, and rarely reach 0.2 mm (e.g. S-41). Most often they are found within wide fractures filled mainly with carbonate, chlorite, or epidote, but they also occur within finer fractures, or along contacts between quartz monzonite and leptite (S-10).

2.3.5. X-Ray Diffraction Analyses of Fracture-Filling Minerals

X-ray diffraction analyses of fractures containing epidote, chlorite, fluorite, pyrite, muscovite (sericite), quartz, and feldspars in samples from an ultra-large core recovered from the 360 m level were obtained (Thorpe et al., 1980). Tables 3 and 4 are diffraction patterns from these analyses, indexed to specific minerals. Patterns were made with a Debye-Scherrer powder camera, Cu K_α radiation, and Ni filter.

In order to index these patterns to prominent d-spacings of the specific minerals, separates enriched in various matrix and fracture-filling minerals were analyzed first. This was necessary because significant variations in d-spacings and relative peak strengths occur in several minerals in response to variations in chemical composition. Samples thus analyzed included separates enriched in quartz, feldspars, and muscovite (i.e., chlorite

Table 3. X-ray diffraction peaks of whole fracture-filling from ultra-large core from the 360 m level (Thorpe and others, 1980).[a]

Strength[b]	2θ (degrees)	d (Å)	d-spacings of minerals (Å)
m-s	8.87-8.90	9.94-9.98	Muscovite 9.95
m-s	12.50-12.53	7.07-7.08	Chlorite 7.05-7.08
w	19.75-19.85	4.473-4.495	Muscovite 4.47-4.48
m-s	20.83-20.90	4.250-4.264	Quartz 4.26
w	22.10-22.13	4.018-4.022	Plagioclase 4.03
s	26.63-26.70	3.339-3.347	Quartz 3.343
w-m	27.75-27.80	3.209-3.215	Plagioclase 3.20 or Muscovite 3.20
w-m	28.08	3.178	Plagioclase 3.18
w	28.30-28.35	3.148-3.153	Fluorite 3.153 or Plagioclase 3.15
w-m	34.90-34.95	2.567-2.571	Muscovite 2.56-2.57
m	36.53-36.58	2.456-2.460	Quartz 2.458
m	39.53	2.280	Quartz 2.282
m	42.43-42.48	2.128-2.130	Quartz 2.128
m-s	47.00-47.05	1.930-1.933	Fluorite 1.931
m-s	50.15-50.18	1.818-1.819	Quartz 1.817
w-m	54.90	1.672	Quartz 1.672
w-m	55.78-55.80	1.647-1.648	Fluorite 1.647
m-s	59.95-60.00	1.542-1.543	Quartz 1.541
m	67.70-67.78	1.383-1.384	Quartz 1.382
m	68.18-68.20	1.375	Quartz 1.375

[a]Dominant minerals are quartz, muscovite (sericite), plagioclase, and flourite. Some chlorite also present. (Composite of 2 readings).

[b]Peaks are designated strong (s), medium (m), or weak (w), as qualitative estimates of line densities in the X-ray photographs. The weakest peaks are not listed.

Table 4. X-ray diffraction peaks of chlorite-enriched separate from
         a thick fracture in the east end of the extensometer drift.

Strength	2θ (degrees)	d (Å)	d-spacings of of chlorites[a] (Å)	
m-s	6.33-6.40	13.8-13.9	(a)	14.1
			(b)	14.0
s	12.50-12.53	7.06-7.09	(a)	7.05
			(b)	7.08
w	18.93-18.95	4.683-4.688	(a)	4.67
			(b)	4.681
s	25.33-25.35	3.513-3.516	(a)	3.52
			(b)	3.523
m	34.30-34.38	2.609-2.614	(a)	2.601
			(b)	2.619
m	34.88-34.98	2.565-2.572	(a)	2.554
			(b)	2.574
m	36.48-36.53	2.460-2.463	(a)	2.454
			(b)	2.469
m	37.43-37.53	2.397-2.403	(a)	2.392
			(b)	2.405
m	39.58-39.63	2.274-2.277	(a)	2.266
			(b)	2.279
m-s	45.00-45.05	2.012-2.014	(a)	2.009
			(b)	2.014
w	48.10-48.15	1.890-1.892	(a)	1.882
			(b)	1.893
s	59.23-59.28	1.559-1.560	(a)	1.551
			(b)	1.560
w	60.83	1.523	(a)	1.513
			(b)	1.523

[a]The letters (a) and (b) designate two varieties of chlorite that have
d-spacings closest to those of Stripa chlorite: (a) thuringite, with some-
what lower d-spacings; (b) bavalite, with somewhat higher d-spacings. Both
these chlorites are somewhat richer in Fe, and poorer in Mg, than the Stripa
chlorite as given in Table 2. Their diffraction patterns and chemical ana-
lyses are taken from the Powder Diffraction File of the American Society
for Testing and Materials, 7-166 (bavalite) and 21-1227 (thuringite).

separated out), one separate enriched in epidote, and another enriched in pyrite.

Samples were prepared for diffraction by grinding, washing, and sieving for the 230-320 mesh (62 μm - 44 μm) fraction. Mineral separates were then obtained by heavy liquid separation in bromoform and/or by use of the Frantz isodynamic magnetic separator.

The error in reading for diffraction films ($\Delta 2\Theta$) is less than $0.1°$. This corresponds to decreasing errors in d-spacing (Δd) with increasing 2Θ (or decreasing d), as follows:

d	Δd (corresponding to $0.1°$ $\Delta 2\Theta$)
14.0 Å	0.22 Å
10.0	0.11
7.0	0.05
3.0	0.01
1.5	0.002

Chlorite analyzed by diffraction in Table 4 is from a wide fracture, and not from alteration of biotite, as was the chlorite analyzed by microprobe in Table 2; it is uncertain whether these are the same or different species of chlorite.

Fluorite, where coarse-grained and a major fracture-filling mineral, is generally clear to pale lavender in thin section. Often it is stained a deeper purple around cracks or opaque grains.

The definitive diffraction peaks used to identify epidote--those peaks not possibly due to other frature-filling minerals--correspond to d = 2.90 Å and d = 2.68 Å. As coarse-grained prisms, epidote is easily identifiable; in thin section, it takes several forms. Often it has low birefringence and other properties that suggest it may be clinozoisite. In many fractures and breccias, epidote is very fine-grained and altered partially or completely to a diffuse, nearly opaque material probably rich in clay. This material is inferred to be epidote by its occasional birefringence, and by its occurrence as an alteration product on edges of otherwise fresh epidote prisms. (Sphene may, in some cases, also be a component of this material).

2.4 Texture of the Stripa Quartz Monzonite

Several textural features of the Stripa quartz monzonite are distinctive. One is the abundance of fractures, both continuous and discontinuous, on a microscopic scale. Even in relatively unfractured samples, fine discontinuous cracks within primary grains or along grain boundaries are very common. These cracks, which are filled with intergrown chlorite and sericite (or muscovite) (Fig. 7), or sometimes quartz and feldspars, suggest several possible interpretations. In some cases they are probably original features of a late stage of primary crystallization, interstitial to earlier formed crystals. But in most cases they are secondary, formed either in the solidified but still cooling quartz monzonite by deuteric or hydrothermal alteration, or much later as a result of heating and deformation unrelated to cooling and crystallization of the pluton. Even in this last case, it is likely that the crack fillings did not crystallize from fluids introduced from extraneous sources, but are due rather to remobilization and redeposition of primary components of the rock matrix. This is suggested by the fact that the

cracks frequently originate among primary grains of the same minerals as those filling the cracks.

This interpretation may be applied to the wider, continuous fractures in the quartz monzonite as well as to the fine, discontinuous cracks. Since the dominant mineralogy of the fracture fillings in general does not differ much from the mineralogy of the alteration products of the primary granitic matrix, it is likely that fractures (with the possible exception of those dominated by carbonate minerals or fluorite) were filled largely as a result of remobilization and recrystallization of primary components. This is of course true as well of fractures that include breccia or microbreccia, where fragments in the breccias are clearly derived from the parent granitic rock.

Another distinctive feature of the Stripa quartz monzonite is the abundance of cataclastic textures, resulting from mechanical deformation. (It should be noted, however, that fractured and brecciated core was chosen preferentially for thin sections, so that the descriptions in Appendix A give an exaggerated impression of the abundance of deformation textures.) Kinked cleavage planes in mica and bent twin lamellae in plagioclase (Fig. 9) are common, and where fracturing is intense these textures give way to granulation and consequent brecciation. Often there is evidence of movement along fracture surfaces or breccia zones. Slickensides are visible on many chloritic open fractures, and some thick fractures are filled with a microscopically irresolvable clay-rich fault gouge enclosing rounded fragments of granitic rock. Also, mylonitic textures, characterized by a foliated groundmass of very finely granulated fragments enclosing scattered aligned augen of

parent rock, occur locally (Fig. 10). These represent an extreme of cataclastic deformation and are rare in the quartz monzonite, present only when adjacent to some dikes or contacts.

2.5 Other Granitic Rocks in the Stripa Region

Outcrops from neighboring granitic plutons--the Gusselby, Dammsjön, and Kloten massifs--have been sampled and studied in relation to the Stripa quartz monzonite. Both texturally and mineralogically these rocks show significant differences from the rock at Stripa. The mineralogy of these plutonic rocks differs from that of the Stripa quartz monzonite in the following respects: there is little or no muscovite; biotite is often abundant, and in most cases chloritization is partial or lacking; hornblende or sphene are often present, and sometimes abundant; apatite is present, as is coarse-grained zircon, and garnet is much rarer than in the Stripa rock, or absent. These differences are apparent in Table 1, showing modal analyses of selected Stripa and other granitic rocks. In Fig. 6, where the same results are plotted in terms of relative abundances of quartz, plagioclase, and microcline, these differences are obscured because the results of the Stripa analyses largely overlap those of the other rocks. However, the differences show up more clearly in comparisons of chemical composition (discussed in the following section).

Neighboring granitic rocks differ texturally from Stripa quartz monzonite in that they are generally coarser-grained, often with large poikilitic microcline, and they are much less pervasively fractured. In general they do not have the fine discontinuous cracks filled with sericite and chlorite, quartz or feldspar characteristic of the Stripa rock. However, the samples from the

Gusselby massif, and two fine-grained light granitic rocks, J 75-14 and
C 75-9, from the Dammsjön and Kloten massifs, respectively, resemble, tex-
turally, the Stripa quartz monzonite.

2.6 Chemical Compositions and Ages of the Granitic Rocks

Three samples of Stripa quartz monzonite, and two samples of neighboring
granitic rocks, were analyzed at LBL for major element abundances by X-ray
fluorescence. The results are shown in Table 5. The silica content of the
Stripa rocks defines them as quartz monzonites rather than "granite" in the
strict sense. Table 6 shows analyses of various samples of neighboring
granitic rocks, determined by the Geological Survey of Sweden (I. Lundström,
private communication). These rocks span a range from true granite (the
relatively high silica rocks) through quartz monzonite, to granodiorite with
relatively low silica contents. These analyses, as well as an average of
nine analyses of Stripa quartz monzonite determined previously (Olkiewicz et
al., 1979) have been computed to normative abundances, and plotted on a
three-component diagram of normative quartz, plagioclase, and K-feldspar
(Fig. 11). In this plot, as in Fig. 6, the fields of Stripa and neigh-
boring granitic rocks overlap, and they are not readily distinguishable.
In Fig. 12, however, where relative oxide abundances of alkalis, Fe, and Mg
are plotted, the Stripa rocks cluster near the alkali corner, reflecting
their paucity of mafic minerals. (One sample from the Gusselby massif,
J 75-1, overlaps the Stripa field, while a second analysis from that outcrop
is much richer in Fe. This discrepancy, as well as others in these analyses,
may be due to heterogeneity of the sampled outcrops).

Table 5. X-ray fluorescence major-element analysis of relatively fracture-free granites from Stripa and neighboring plutons.

Oxides	Stripa Quartz Monzonite			Gusselby Massif	Kloten Massif
	E7-2[a]	S-12	S-38	J 75-1	I 75-11
SiO_2	73.83 ± 1.48	74.73 ± 1.49	74.37 ± 1.49	72.29 ± 1.45	67.60 ± 1.35
TiO_2	~ 0.3 ± 0.2	~ 0.03 ± 0.2	~ 0.06 ± 0.2	~ 0.4 ± 0.2	~ 0.6 ± 0.2
Al_2O_3	14.24 ± 0.28	13.91 ± 0.28	14.12 ± 0.28	13.64 ± 0.27	13.87 ± 0.28
Fe_2O_3[b]	1.07 ± 0.02	1.20 ± 0.02	0.92 ± 0.02	2.93 ± 0.06	5.89 ± 0.12
MnO	~ 0.03 ± 0.02	~ 0.04 ± 0.02	~ 0.03 ± 0.02	~ 0.07 ± 0.02	~ 0.14 ± 0.02
Cr_2O_3	< 0.05	< 0.05	< 0.05	< 0.05	< 0.05
MgO	~ 0.2 ± 0.7	~ 0.2 ± 0.7	~ 0.3 ± 0.7	~ 0.4 ± 0.7	~ 0.7 ± 0.7
CaO	0.85 ± 0.02	0.81 ± 0.02	0.79 ± 0.02	1.30 ± 0.03	2.42 ± 0.05
Na_2O	4.14 ± 2.1	3.51 ± 1.8	4.13 ± 2.1	3.39 ± 0.17	3.26 ± 0.16
K_2O	4.65 ± 0.09	4.90 ± 0.10	4.29 ± 0.09	5.22 ± 0.10	4.84 ± 0.10
Total	99.0	99.3	99.0	99.7	99.3

[a]Average of two analyses. This sample is from an extensometer hole drilled from full-scale drift.

[b]Total Fe as Fe_2O_3. Oxidation state of Fe unknown.

These whole rock chemical analyses were obtained at LBL on a multiple anode soft X-ray fluorescence spectrometer (Hebert and Street, 1973). The sample was first ground to a fine powder, then fused with a $LiBO_2$ flux and poured to form a glass disc.

Errors are computed as 2% of reported values for relatively abundant oxides, except for Na_2O for which a 5% error is used. This corresponds roughly to one standard deviation. For oxides of very low abundance, values are more approximate.

Table 6. Whole-rock chemical analyses of granitic rocks from other plutons in the Stripa region; data provided by I. Lundström of the Geological Survey of Sweden.

Oxide				Kloten Massif				Gusselby Massif			Dammsjön Massif		
	C75:9	C75:10	C75:11	I75:10	I75:11	I75:22	IL79:1 I75:16	J74:1	J75:1	J75:4	J75:7	J75:8	J75:9
	%	%	%	%	%	%	%	%	%	%	%	%	%
SiO_2	76.1	74.5	72.6	75.2	69.8	74.0	77.8	71.5	74.1	71.3	72.3	70.0	71.9
TiO_2	0.11	0.30	0.44	0.13	0.73	0.34	0.08	0.36	0.03	0.58	0.37	0.63	0.53
Al_2O_3	12.9	13.0	13.0	12.9	13.6	13.3	13.0	13.8	14.2	13.4	13.1	13.6	13.1
Fe_2O_3	1.4	3.2	4.0	2.0	5.8	3.4	1.2	2.4	0.9	4.3	3.5	4.9	4.8
MnO	0.01	0.04	0.05	0.05	0.09	0.05	0.02	0.04	0.03	0.08	0.06	0.09	0.07
MgO	0.20	0.17	0.28	0.39	0.76	0.32	0.19	0.48	0.09	0.62	0.32	0.68	0.49
CaO	0.6	1.2	1.6	1.0	2.3	1.3	1.4	1.1	0.4	1.7	1.6	2.1	1.4
Na_2O	3.2	3.0	3.0	3.5	2.9	3.2	3.8	3.2	4.2	3.3	3.5	3.4	3.1
K_2O	5.2	5.2	5.3	4.6	4.8	5.0	3.4	5.6	5.6	4.7	4.7	4.4	4.7

NORMS

Qz
60

STRIPA PLUTON
① S-12
② S-38
③ E 7-2
Ⓐ Average of 9
analyses

GUSSELBY MASSIF
① J74·1
◯ 2a J75·1
◯ 2b J75·1

Ⓐᵥᵍ "regional average"

KLOTEN MASSIF
1 C-75·9
2 C-75·10
3 C-75·11
4 I 75·10
5a I 75·11
5b I 75·11
6 I 75·22
7 IL 79·1

DAMMSJÖN MASSIF
△ J·75·4
△ J·75·7
△ J·75·8
△ J·75·9

40

7 7

1

2 4

3

6

Avg Ⓐ ② 2

5a

① 2b

3 3

2a 5b

20
Kspar

40

60
Plag

weight percent

XBL 814-9188
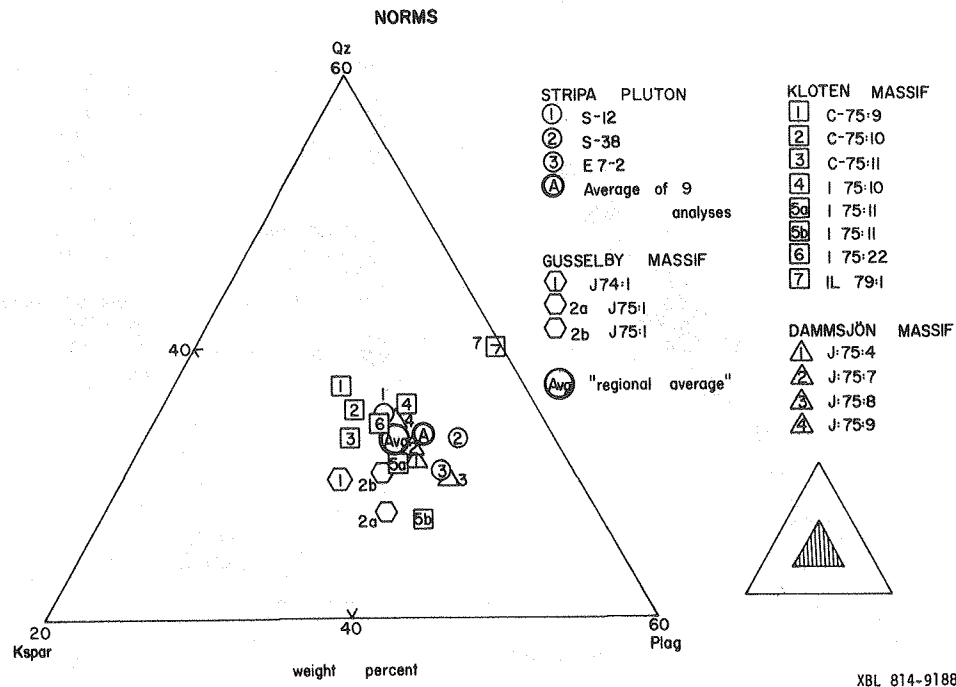
Fig. 11. Relative normative abundances of quartz, plagioclase, and K-feldspar (normalized to 100%) in analyses listed in Tables 5 and 6, and in nine analyses of Stripa quartz monzonite by A. Olkiewicz et al. (1978).
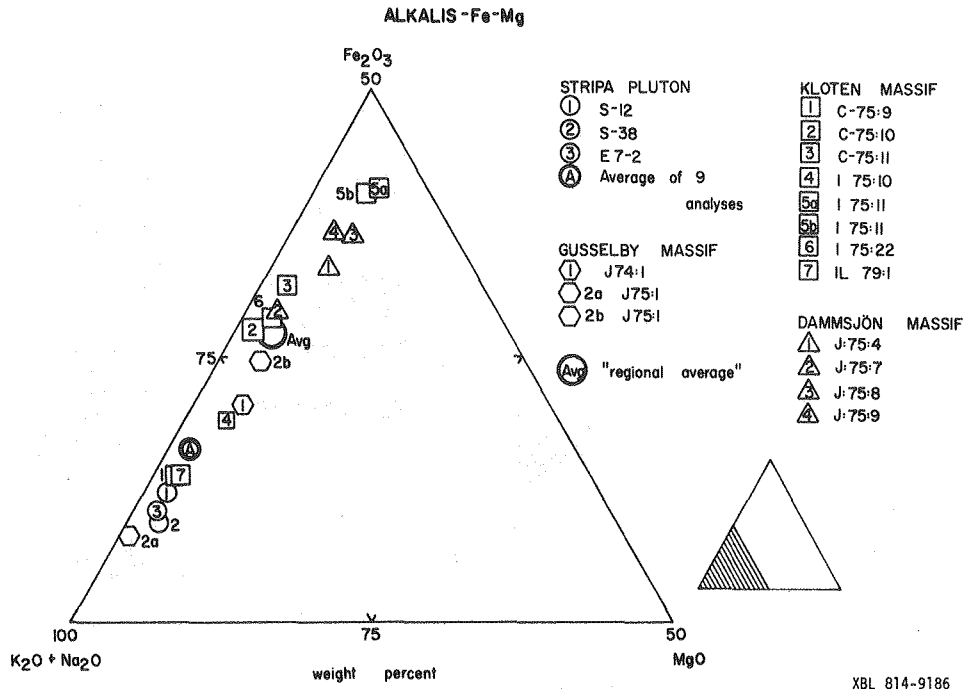
Fig. 12.   Relative abundances of oxides of Fe, Mg, and
           alkalis (normalized to 100%), in samples in
           Fig. 11.

Radiometric dates for one sample of Stripa quartz monzonite (S-38)
and two of neighboring granitic rocks, J 75-1 (Gusselby massif) and I 75-11
(Kloten massif), were determined by potassium-argon dating at the University
of California, Berkeley, by G. Curtis and R. Drake. For the Stripa sample, a
muscovite separate was used; for the others, biotite separates. The samples
showed little or no alteration of the mica minerals, and the coarse sieve
fraction of the separates should have excluded most secondary fine mica
grains filling fractures or discontinuous cracks.

The dates obtained in these analyses were, in millions of years,
1691 ± 16, 1604 ± 14, and 1640 ± 44 for S-38, J 75-1, and I 75-11, respec-
tively (Table 7). As muscovite has a slightly higher argon retentivity than
biotite, the gap between the oldest (muscovite) date and the youngest date
would be smaller than these figures indicate. Despite precautions taken to
ensure that the separates were free of micas of clearly secondary origin,
there is no assurance that these dates represent the true ages of primary
crystallization and original argon retention or that they were not reset by a
later thermal event.

For comparison, Welin et al. (1980) reported older K-Ar ages of musco-
vite (1712 to 1826 m.y.) from late kinematic stage pegmatites of the Uppsala
region. Silicic volcanic rocks in the Uppsala region have a significantly
higher whole-rock Rb-Sr age of 1830 m.y.

2.7 Leptite and Associated Rocks

Leptite is a common rock both in outcrop and in cores from Stripa.
It is usually a grey-green to black, fine-grained foliated metamorphic

Table 7. Results of radiometric dating of granitic samples from the Stripa region, by the potassium-argon method.

Sample	Mineral Analyzed	$^{40}Ar*$ (ppm)[a]	$^{40}Ar*/^{40}Ar$ Total[a]	K(%)	Date (in 10^6 years)[b]
S-38 (Stripa)	muscovite	4.331×10^{-2}	0.990	8.911 ± 0.1	1691 ± 16
J 75-1 (Gusselby Massif)	biotite	3.234×10^{-2}	0.983	7.214 ± 0.1	1604 ± 14
I 75-11 (Kloten Massif)	biotite	2.760×10^{-2}	0.312	5.953 ± 0.1	1640 ± 44

[a] $^{40}Ar*$ refers to radiogenic ^{40}Ar; ^{40}Ar Total is the sum of radiogenic and atmospheric ^{40}Ar.

[b] Error in dates depends on error in K abundance, and on ratio of atmospheric to radiogenic ^{40}Ar.

Constants:

$$\lambda_\beta = 4.962 \times 10^{-10}/year$$

$$\lambda_e + \lambda_e' = 0.581 \times 10^{-10}/year$$

$$^{40}K/K_{total} = 1.167 \times 10^{-4}$$

Muscovite and biotite separates used for these analyses were obtained by crushing, sieving for the 28-60 mesh fraction (295 - 589 μm), and separation by the Frantz isodynamic magnetic separator.

Analyses by R. Drake and G. Curtis, and potassium analyses by flame photometry by J. Hampel, of the Department of Geology and Geophysics, University of California, Berkeley.

rock (microschist) often cut by white or light green fractures. Minera-
logically it is similar to the Stripa quartz monzonite; it is composed mainly
of quartz, plagioclase, microcline, chloritized biotite, and muscovite. But
texturally, it does not resemble most of the granitic rocks, as it is much
finer, more even-grained, and homogeneous (Fig. 13).

In detail, leptites generally consist of a fine, even-grained mosaic of
equant quartz grains with fewer plagioclase and microcline grains. Parallel,
elongate laths of chlorite and muscovite define the foliation. Sub-equant
quartz porphyroblasts*, typically up to 1-2 mm in diameter, are common
(Fig. 13). Darker leptites generally contain more chlorite, at the expense
of muscovite, than the lighter leptites, or they contain fewer porphyro-
blasts. As in the Stripa quartz monzonite, chlorite has generally replaced
biotite completely, but in a few cases some biotite remains intergrown.
Pleochroic halos are common within chlorite and may contain discrete
opaque grains or, rarely, birefringent high-relief grains, probably zircon
(e.g., ST-27). Muscovite, like chlorite, generally occurs in narrow laths,
but coarser muscovite also occurs and is generally sieve-textured.

Fractures are abundant in the leptite, and fracture-fill mineral-
ogy is similar to that in the quartz monzonite. Epidote, however, appears to
be more abundant in the leptite than in the quartz monzonite, commonly
filling light green sinuous fractures up to 1 cm wide. Coarse prisms of
epidote are the sole constituents of some fractures, while in others epidote
is intergrown with quartz, with sericite and chlorite, or with carbonate

---

*The term "porphyroblast" is intended here in a descriptive sense only.
Regarding the origin of the porphyroblasts, the consensus among Swedish
geologists is that they are relict phenocrysts, and that the leptites are
metamorphosed volcanic and volcanistic rocks (Olkiewicz et al., 1979; Geijer
and Magnusson, 1944).
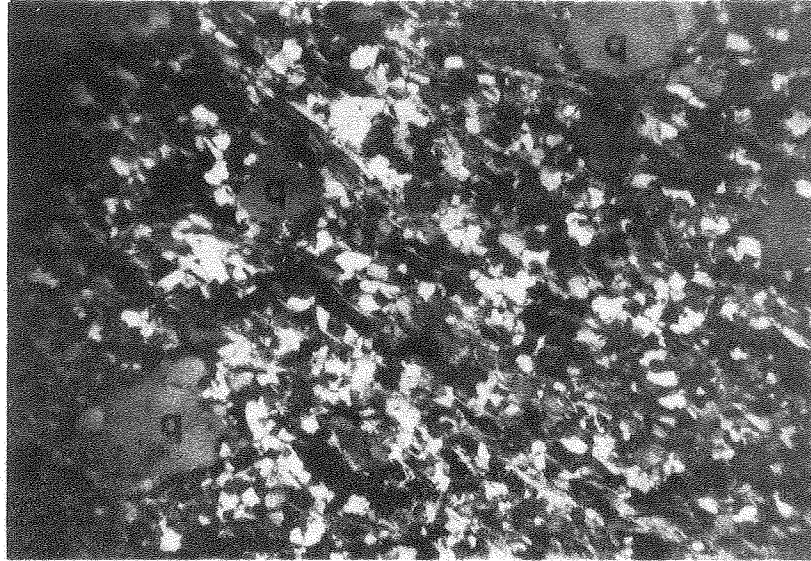
0.5 mm   XBB 800-13602A

Fig. 13. Fine-grained foliated leptite, ST-1. Foliation
          (diagonal from upper left) is defined by narrow
          laths of muscovite and lesser chlorite, set in
          an even-grained mosaic of quartz, microcline,
          and plagioclase. Small quartz porphyroblasts (q)
          are present. Cross-polarized light.

minerals and fluorite. Epidote also occurs in isolated patches in leptite, and in some cases as prisms aligned parallel to the foliation. Quartz-filled or quartz-carbonate-filled fractures are also abundant, and in several thin sections may be seen to cut and offset epidote veins (Fig. 14). Chlorite occurs as a fracture-filling mineral, but much less abundantly than in the quartz monzonite. Brecciated leptite occurs in wide fracture zones (e.g., S-6), with interstices between fragments filled with coarse grained fluorite, carbonate, quartz, and other minerals. Finely brecciated leptite (microbreccia) is an occasional constituent of wide fractures. Also, very fine intergrowths of quartz and feldspars, with lesser chlorite, sericite, and opaque materials, commonly form vein-like features in leptite. It is unclear whether these are fracture fillings or simply textural inhomogeneities within the leptite matrix.

Leptites have been interpreted as originating from rhyolitic lavas and tuffs, possibly deposited in water (see footnote, p. 39). In the leptites studied here, textures that would indicate a volcanic protolith have generally been erased by metamorphism. They generally resemble schists derived from shale or sandy shale, thus suggesting a volcaniclastic protolith.

Contacts of leptite with Stripa quartz monzonite have been observed in several thin sections, and these contacts are generally sharp. Thin growths of sericite, or epidote-chlorite-filled fractures, sometimes occur at the contact; in one case (S-17) uranium-bearing opaque grains are associated with the contact.

Contacts between quartz monzonite of typical Stripa texture and more even-grained foliated granitic rock resembling leptite were observed in

0.5 mm   XBB 800-13608A
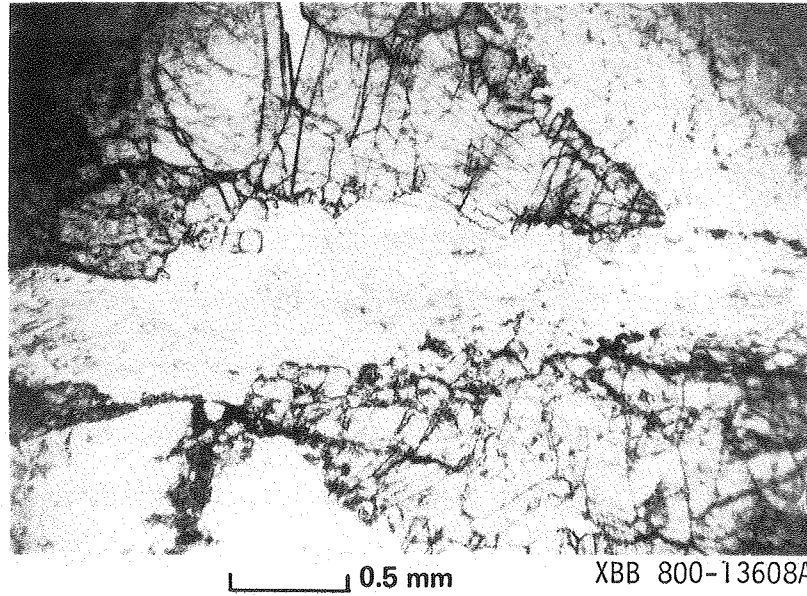
Fig. 14. Intersecting fractures in leptite, S-5. Fracture
          filled with quartz and carbonate mineral (horizontal
          in figure) offsets wider epidote-filled fracture
          (diagonal from upper left). Sense of offset is
          left-lateral. Plane-polarized light.

several thin sections (e.g., S-44, S-45). In one sample (S-10) a band of foliated granitic rock, 1 mm wide, separates quartz monzonite from a thick foliated, chlorite-rich fracture zone. This thin band contains abundant chlorite grains in parallel alignment and is essentially a leptite; yet it is gradational from quartz monzonite of more typical texture. This points up the occasional difficulty of distinguishing foliated granitic rock from leptite in hand sample.

2.8 Amphibolite and Diabase

Another variety of metamorphic rock at Stripa is a dark green, fine-grained foliated rock rich in blue-green prismatic amphibole, often logged in core descriptions as "greenstone." Texturally this amphibolite is a micro-schist like the more abundant leptite. However, its foliation is determined by amphibole prisms instead of chlorite and muscovite laths. Interstices between amphiboles consist of quartz, plagioclase (very altered), opaques, and carbonate. White fractures filled mainly with carbonate and quartz, and light green fractures filled mainly with epidote, are common in the amphibolite. Also, wide foliated fracture zones occasionally cut amphibolite (S-9), and these contain lenses of various colors and materials aligned parallel to the foliation. Carbonate is last in the sequence of these fracture-filling materials (Fig. 15). One sample of dark, mafic rock (S-14) does not have a foliated, schistose texture, but consists, instead, of much coarser, stubby amphibole grains. In hand sample it resembles an altered diorite, but can be seen in core samples to grade into the more typical amphibolite.

0.5 mm   XBB 800-13727A
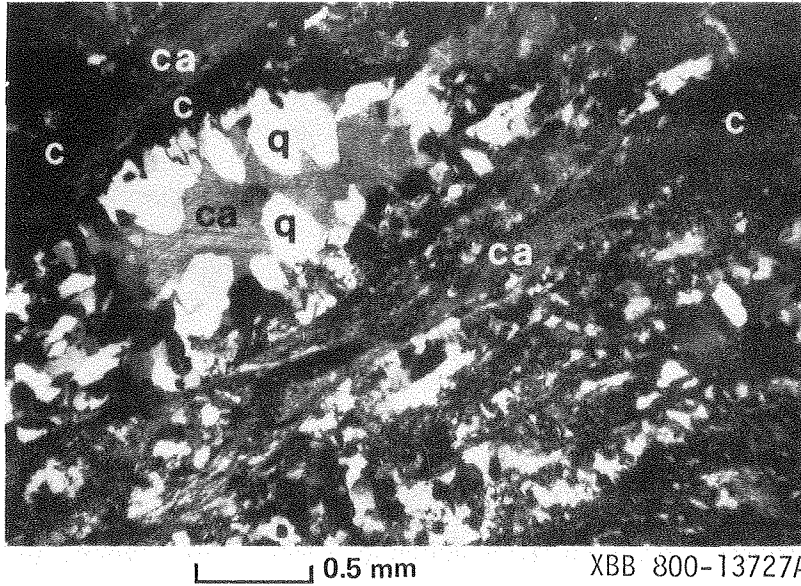
Fig. 15. Wide foliated fracture zone in amphibolite, S-9.
          Lensoid cavity at upper left is lined with quartz
          euhedra (q), and filled with carbonate mineral
          (ca) deposited over the quartz. It is bordered
          by bands of chlorite (c) and fine-grained car-
          bonate. Lower right portion of figure consists
          of a fine breccia of fragmented quartz and feldspar
          grains with intergrown chlorite, sericite, and
          carbonate. Cross-polarized light.

Some Swedish geologists have interpreted amphibolite dikes as being altered diabase (Olkiewicz et al., 1979). Our observations of a limited number of amphibolite samples at Stripa neither support or reject this interpretation.

One sample of altered diabase (ST-35) was examined in thin section and is described in detail in Appendix A. It resembles a dark leptite in hand sample, but has an even more uniform grain size, and is not foliated.

3.0 RADIOGEOLOGY

The abundance of radioelements was measured, both on the surface and underground, to obtain a preliminary indication of the geochemical homogeneity of the Stripa pluton and to calculate its radiogenic heat production.

3.1 Instrumentation

The instrument used to determine the concentrations of the radioelements --potassium, uranium and thorium--was a portable gamma-ray spectrometer (GR-410) with a scintillation detector (GPX-21), both made by Geo-Metrics Inc. The detector consists of a 3-in. diameter by 3-in. thick thallium-activated sodium-iodide crystal optically coupled to a high-gain photo-multiplier tube that is hermetically sealed within a thermally insulated housing. The housing contains a high-voltage power supply and a pre-amplifier.

The K, U, and Th concentrations are calculated from counts accumulated by the γ-ray spectrometer in three pre-set intervals of the γ-ray energy spectrum, centered respectively on the ^{40}K peak at 1.46 MeV, the ^{214}Bi peak at 1.76 MeV, and ^{208}Tl peak at 2.62 MeV. The widths of the K and Bi intervals are 200 KeV, and that of the Tl interval is 400 KeV. As ^{214}Bi and ^{208}Tl are the respective daughter products of the ^{238}U and ^{232}Th decay series, it is assumed that they are in secular equilibrium with their parents in the rocks being measured. A fourth interval, total counts, encompasses a broad portion of the γ-spectrum, from 0.5 to 5.0 MeV.

3.2 Field Procedures

A total of 81 gamma-ray readings were made, at both surface and underground locations (see Figs. 1-4 for locations). All measurements were made with the detector held in contact with the rock. Three different recording times were used, depending on the counting rates observed: 20 seconds at sites of high γ activity, 1 minute at sites of intermediate activity, and 2 minutes at relatively low-activity sites. The counting times were chosen to allow a statistically significant number of counts to accumulate in the lowest-radioactivity interval, that of ^{208}Tl. The count rates for the three radioelements, the total counts, and the measurement time were recorded. A hand specimen, for subsequent laboratory tests, was taken at almost every sample location.

3.3 Treatment of Field Data to Yield the K, U and Th Values

Before any data were taken, the gamma-ray spectrometer was calibrated with the internal reference isotope (^{133}Ba) with a γ-ray energy of 0.355 MeV, using a split window and a gain adjustment potentiometer. The instrument's background count rates, measured in a low-background environment at Lawrence Livermore National Laboratory, were:

Total counts: 2004 counts/minute

Potassium interval: 20.8 counts/minute

Uranium interval: 26.4 counts/minute

Thorium interval: 9.6 counts/minute

These numbers were then subtracted from the field readings to get a "net count rate" for each energy interval. Two different sets of equations

were used to derive the radioelement concentrations from the count rates: one
provided by the manufacturer, Geometrics Inc., based on measurements at the U.S.
DOE facility at Grand Junction, Colorado, and one obtained from measurements
on pads of known radioelement content at Risø National Laboratory, Denmark as
follows:

(a) From the manufacturer:

Potassium (%) = $[C_K - 0.68C_U - 0.83C_{Th}]/$ 154

Uranium (ppm) = $[C_U - 0.62C_{Th}]/20.5$

Thorium (ppm) = $C_{Th}/7.5$

where C_K, C_U and C_{Th} are the "net count rates" in counts per minute for
potassium, uranium and thorium, respectively.

(b) From Risø National Laboratory:

Potassium (%) = $[C_K - 0.51C_U - 0.86C_{Th}]/161$

Uranium (ppm) = $[C_U - 0.59C_{Th}]/15.9$

Thorium (ppm) = $C_{Th}/7.0$

The differences between the two sets of equations are most likely due to
the different physical characteristics of the DOE and Risø standards.

3.4 Laboratory Gamma Spectrometry Results

To provide definitive calibration for the portable Y-spectrometer data,
14 of the hand specimens were analyzed by A. Smith in the LBL low background
counting facility. The hand specimens were chosen from both surface and sub-
surface locations and included all rock types encountered at Stripa. The
results of by laboratory Y spectrometry are given in Table 8.

After the apparent radioelement concentrations were calculated from the
above equations, we attempted to obtain more nearly actual values by

Table 8. Laboratory γ-spectral analyses of Stripa rock types.

Sample No.	Locality No.[a]	Description	U (ppm)	Th (ppm)	K (%)
ST-1	γ7	leptite, surface	2.25	11.1	3.63
ST-3	γ9	qtz. monz., surface	24.4	31.3	3.98
ST-9	γ39	qtz. monz., underground	34.2	32.1	3.97
ST-12	γ42	qtz. monz., underground	40.9	31.4	3.84
ST-18	γ20a	qtz. monz., abundant chlorite, underground	44.1	31.2	4.14
ST-18a	γ20b	qtz. monz., underground	42.8	31.3	3.77
ST-21	γ32	qtz. monz., underground	35.2	29.2	3.75
ST-27	γ54	leptite, underground	6.10	17.2	2.72
ST-32	γ12	leptite, surface	3.63	11.2	2.15
ST-35	γ34	diabase, underground	1.19	3.79	1.28
ST-48	γ68	reddish granitic, surface	15.4	30.5	3.99
ST-23	γ47	uranium ore, underground	1320	22	--
ST-23a	γ47	banded Fe ore, underground	0.51	0.35	0.003

a Gamma measurement locality number.

plotting the laboratory-determined radioelement contents against the field re-
sults for the same samples (from both underground and surface locations); the
calibration curves are shown in Fig. 16. The slopes and intercepts of the
lines were then used to correct the field readings. These corrected values
are listed in Appendix B and summarized in Table 9.

The calibration diagrams (Fig. 16) indicate that the slopes of the lines
relating laboratory analyses to surface measurements are considerably steeper
than those relating laboratory to underground measurements. This is because
the underground sites are essentially surrounded on all sides by γ sources
(~ 4 π geometry) in contrast to the surface where planar geometry predomin-
ates. The high zero intercept on the calibration diagram for underground
measurements of uranium may be attributed to the abundance of radon in the
mine's air. The low background indicated in the thorium interval for under-
ground measurements is attributed to the attenuation of cosmic rays by the
rock, resulting in a lower contribution of counts to the Th interval from high-
energy cosmic rays than at the surface. Calibrations based on the Risø and
DOE facilities are most applicable to the geometry of surface measurements.

3.5 Fission Track Radiography Results

The fission-track radiographic method (Wollenberg, 1972) was used to deter-
mine the location and abundance of uranium in uncovered thin sections. Most
samples were of Stripa quartz monzonite, but also included where three leptites
and several neighboring granites.
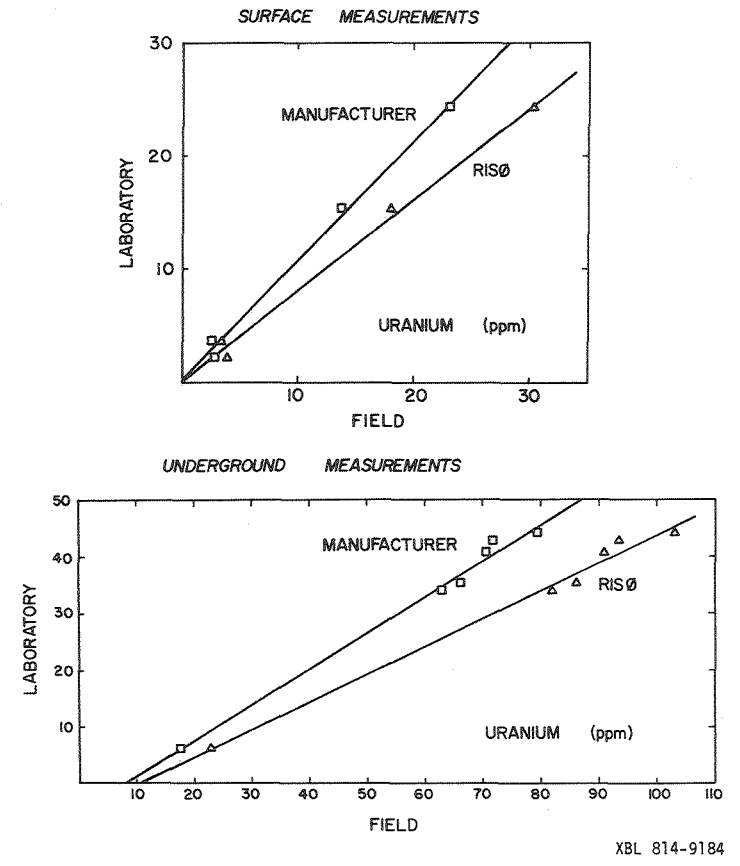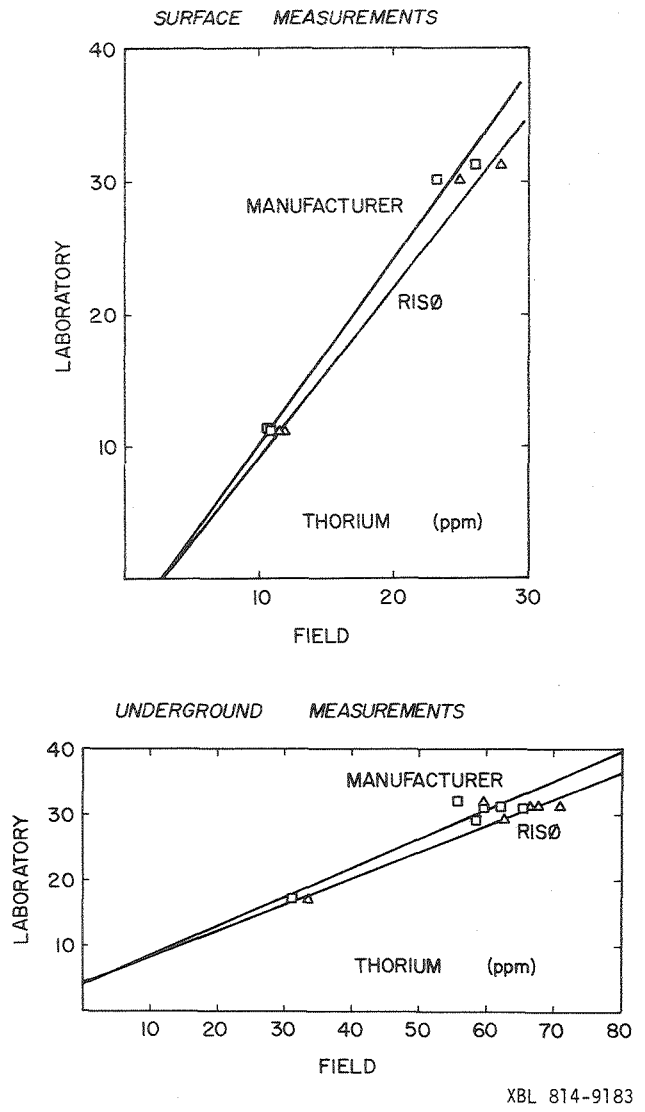
Fig. 16. Calibration curves relating radioelement contents determined by surface and underground γ-spectral measurements to laboratory radioelement analyses.

Table 9. Mean and standard deviation of radioelement contents.

Rock Type	No. of meas.	U, σ (ppm)	Th, σ (ppm)	K, σ (%)	Th/U	Radiogenic Heat Production	
						(cal x 10^{-13} cm^{-3} sec $^{-1}$)	(μ Wm^{-3})
Stripa Qtz. Monz.[a]							
Surface	9	26.9, 5.5	33.0, 5.7	4.6, 0.7	1.1, 0.1	23.3, 4.5	9.5
Underground	34	37.4, 6.2	29.2, 3.8	3.9, 0.3	0.8, 0.1	29.4, 4.0	11.9
Leptite[a]							
Surface	5	3.3, 0.7	11.9, 2.9	3.1, 0.6	3.6, 0.4	4.8, 0.8	1.95
Underground	9	5.4, 3.1	17.9, 1.4	2.8, 0.5	3.9, 1.2	7.1, 0.7	2.9
Regional Granitic Rocks[a]	7	17.6, 15.4	26.6, 6.6	5.2, 1.5	2.4, 1.2	16.6, 10.5	6.8
Malingsbo Granite[b]	67	15.7, 14.9	38.6, 20.6	4.0, 0.7	3.2, 1.6		7.1
Regional Metamorphic Rocks[a]	5	6.1, 1.5	14.6, 8.7	2.5, 1.1	2.6, 1.9	6.9, 1. 7	2.8

[a] By gamma-spectrometric field measurements.

[b] From Landström et al.(1979), determined by laboratory analysis.

In the Stripa quartz monzonite, uranium is most highly concentrated
in tiny opaque grains about 50 μm or less in diameter, often euhedral, and some-
times square in cross-section. These grains are usually found in chlorite,
but also in muscovite-chlorite-sericite-filled fractures, and even in cracks
within quartz or feldspar (Figs. 17 and 18). The grains often contain up to
10-20% U, but concentrations greater than 50% U have been observed. In
chlorite, these grains are surrounded by deep pleochroic halos, and where
they occur in quartz or feldspar they occasionally will also have dark halos
around them, possibly a result of alteration due to radiation damage.
Although pleochroic halos are very abundant in chlorite grains, they are not
a reliable indicator of U loci; in fact, they only rarely include uranium-rich
opaque minerals.

Another locus of uranium concentration is in opaque grains of a differ-
ent morphology and mode of occurrence. These grains are larger--from 0.2 to
0.5 mm--and they are anhedral, often with irregular, scalloped edges, in
contrast to the frequently euhedral opaques discussed above. Uraniferous
anhedral opaques have been observed in two samples. One is a contact between
quartz monzonite and leptite (S-17); here anhedral opaques occur in a quartz-
epidote-sericite-filled fracture on the contact, and on fine carbonate-sericite
stringers intersecting the contact on the quartz monzonite side (Fig. 19).
The other sample is a network of fractures in quartz monzonite, filled with
calcite and asphaltite (see discussion in Section 2.3.1); anhedral opaques
are abundant in this sample, and occur both within and adjacent to the frac-
tures. In both samples, the uraniferous opaque grains contain ~ 1-3% U.
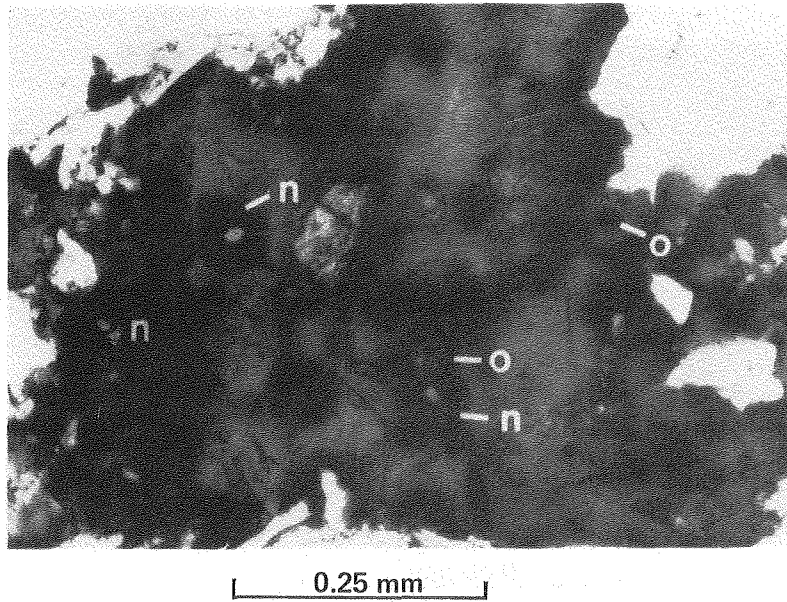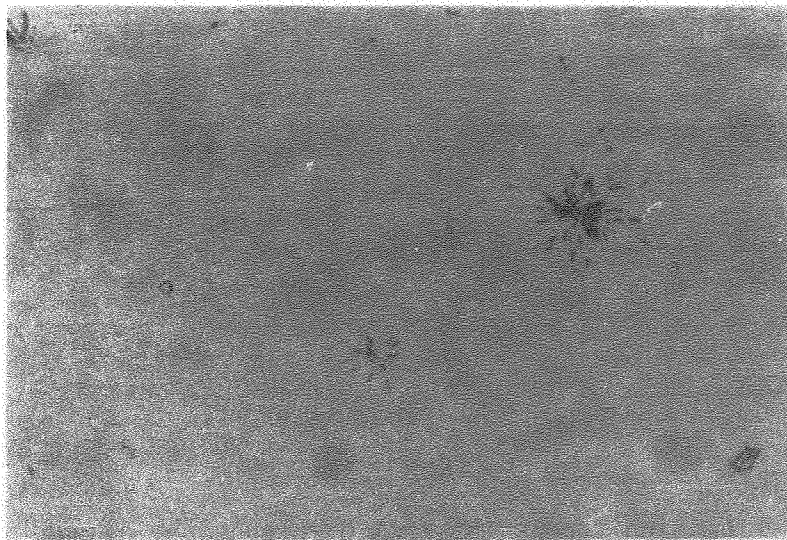
Fig. 17. Fission tracks (B) from U in two fine opaque grains (o)
in chlorite (A), in relatively unfractured quartz
monzonite, S-38. U concentration in these grains is
>50%. Note several non-opaque grains (n) which, although
enclosed in pleochroic halos like the opaque grains, lack
associated fission tracks. The edges of the chlorite
grain also have sparse fission tracks associated. Plane-
polarized light.
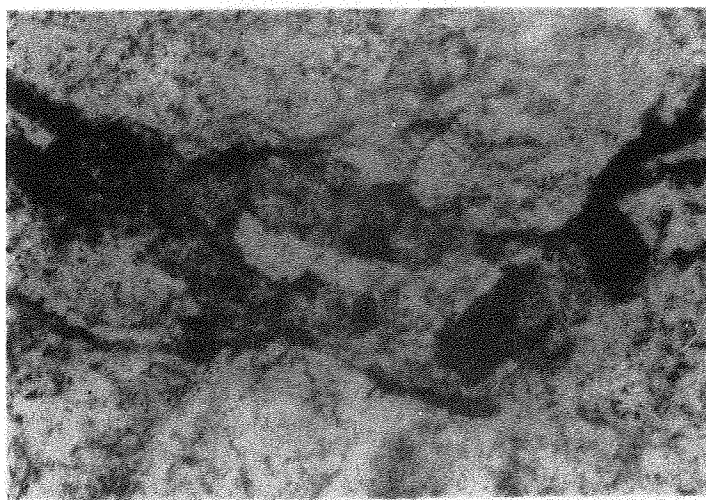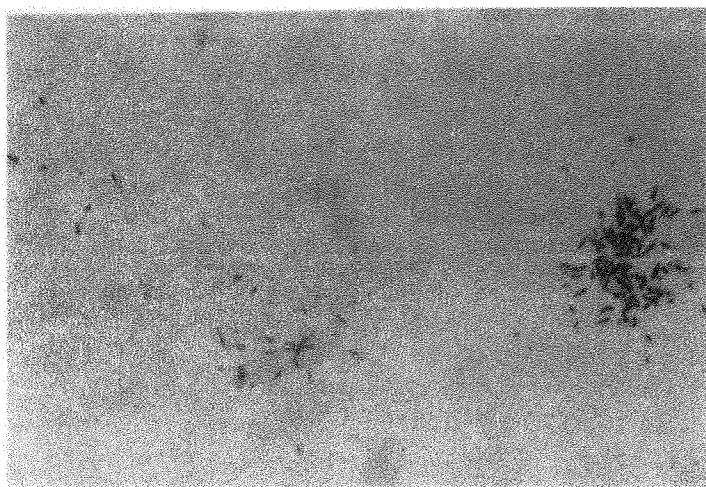
Fig. 18. Fission tracks (B) from U in euhedral opaque
grain (20-30% U), and along fine chlorite-
filled fractures (0.5 to 1% U) in fractured
and brecciated quartz monzonite, S-29 (A).
Plane-polarized light.
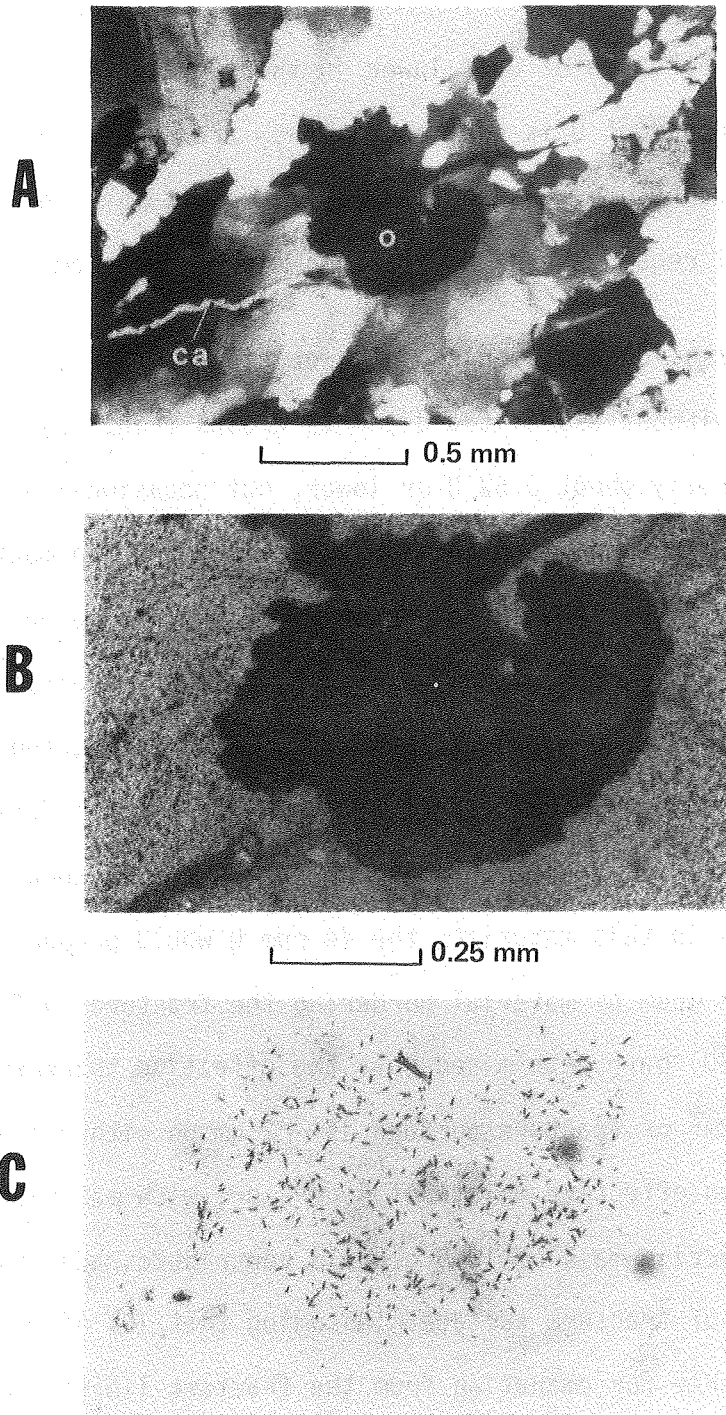
Fig. 19. (A) Anhedral opaque grain (o) on carbonate stringer (ca) in fractured granitic rock adjacent to contact with leptite, S-17. Cross-polarized light. (B) Same grain at higher magnification. (C) Fission tracks from U (~2%) in opaque grain of (A) and (B). Plane-polarized light in (B) and (C).

Although the concentration of U is lower in these grains than in the euhedra, the absolute abundance of U is greater, as they are larger in volume by well over an order of magnitude. Proper identification of the mineralogy of the opaque grains will require detailed electron-microprobe examinations.

Uranium is also found dispersed in lower concentrations along chlorite-filled fractures without associated discrete grains (Fig. 18). Concentrations are generally about 0.5% U or lower, but occasionally range up to about 1.0% U. Uranium concentrations in these loci are the most likely sources of the ^{222}Rn observed by Nelson et al. (1980) in water in some of the Stripa boreholes. A laboratory gamma-spectrometric analysis on this type of fracture coating in the extensometer drift (ST 18) indicated a whole-rock U content of 44 ppm, significantly higher than the mean for Stripa quartz monzonite (Table 9). If uranium daughter products are in secular equilibrium with their parents in this material, the 44 ppm U would produce $\sim 1 \times 10^{-16}$ grams of ^{222}Rn per gram of material bordering the fracture surface. Nelson et al. (1980) have determined that the effective thickness for radon emanation from 1 cm^2 of fracture surface is ~ 2 cm on either side of the fracture. Thus, an effective volume of 4 cm^3, or, with material of density 2.6 g/cm^3, an effective mass of 10.5 g would contribute radon to each square centimeter of fracture surface. Assuming that 10% of the ^{222}Rn produced is available for emanation from the fracture lining, this would provide $\sim 10.5 \times 10^{-17}$ grams of ^{222}Rn to the fracture water from each square centimeter of surface material, or ~ 16 picocuries of ^{222}Rn per square centimeter. Higher U concentrations would produce proportionately greater amounts of radon.

Fission-track radiography of samples of Stripa leptite supports, with some exceptions, the conclusion derived from γ-spectrometric measurements that the leptite contains a much lower uranium concentration than the quartz monzonite. For instance, in one sample of fractured leptite, S-5, no appreciable discrete concentrations of uranium were observed, either in the matrix or in a coarse epidote-filled fracture cutting it. On the other hand, another sample, S-6, a fractured and brecciated leptite, contains uranium concentrations of from several percent up to 20% in several very fine opaque grains, some euhedral, in and adjacent to chlorite, epidote, or carbonate minerals. In addition, uranium concentrations of several percent occur in cracks, with no discrete grains associated, in fracture-filling fluorite in this sample. (The flourite in these fractures, and also adjacent to uraniferous opaque grains, is usually colored a deep purple. Purple fluorite, however, is not always associated with uranium.)

Samples of the neighboring granitic rocks have lower concentrations of uranium than the Stripa quartz monzonite, with U-rich opaque grains rare or absent. One sample (J75-14) contains a dense locus of fission tracks associated with uranium in a fracture filled largely by (and obscured by) hematite, while another sample contains significant uranium associated with a non-opaque grain, possibly metamict zircon.

Uranium minerals have been observed in chlorite-filled fractures cutting the iron ore at Stripa (Welin, 1964). The U content of this fracture material ranges from a few tenths of a percent (sample ST-23) to ore-grade concentrations as high as a few percent. A detailed examination of the distribution and abundance of U within these fractures and in the wall rock

adjacent to and away from the fractures, using the fission-track method, may be a good "natural analogue" to the transport and diffusion of U from a discrete source into a crystalline rock matrix.

3.6 Discussion of Radioelement Data

3.6.1 Relative Abundances

The Stripa quartz monzonite is unusual for its abundance of radioelements and their ratios. Table 9 indicates the relatively high uranium and thorium contents of the quartz monzonite, compared with other plutons measured in the region as well as with the nearby Malingsbo granite, analyzed for radioelements by Landström et al. (1979). Figure 20, the triangular diagram relating the corrected abundances of U, Th, and K measured by field gamma spectrometry, shows distinct radioelement fields for the Stripa pluton, compared with leptite and other granitic rocks in the region. An indication of the relatively high content of the Stripa quartz monzonite is the Th/U ratio, which is considerably lower (1.2 in surface and 0.8 in subsurface exposures) than the average of 2.6 measured in most other granitic rocks in the region, the ratio of 3.2 in Malingsbo granite (Landström et al., 1979), or the range of 2 to 4 in granitic rocks in general. Only two measurements in other plutons--reddish "granite" in exposures north of Gränshyttan (locations 9 and 10, Fig. 1a)--contain relatively high uranium, similar to Stripa quartz monzonite.

3.6.2 Variation with Depth

Table 9, the abundance diagram of Fig. 20, and the plot of Th and U versus depth in the quartz monzonite (Fig. 21)--all indicate that uranium is depleted in surface exposures of quartz monzonite and leptite at Stripa, relative to its
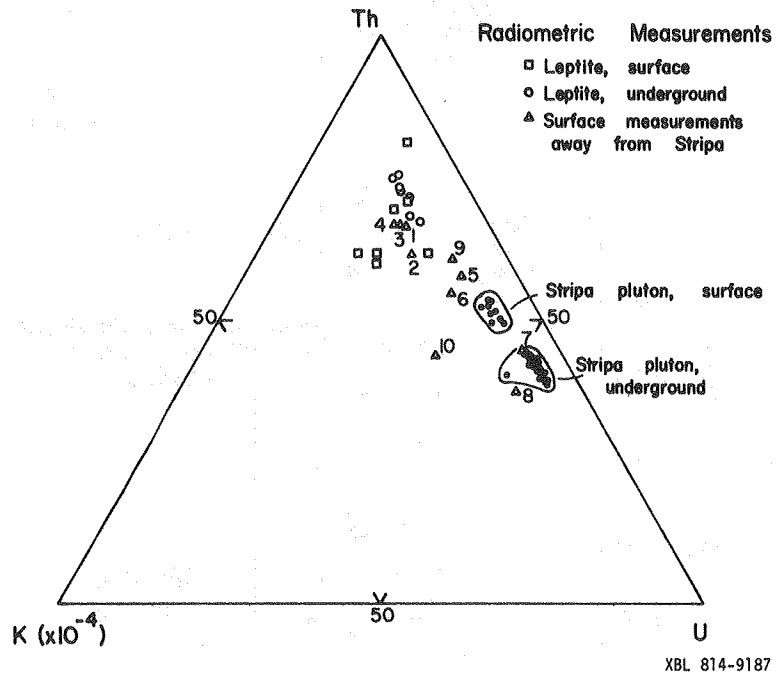
Fig. 20. Triangular diagram showing relative abundances of radioelements.
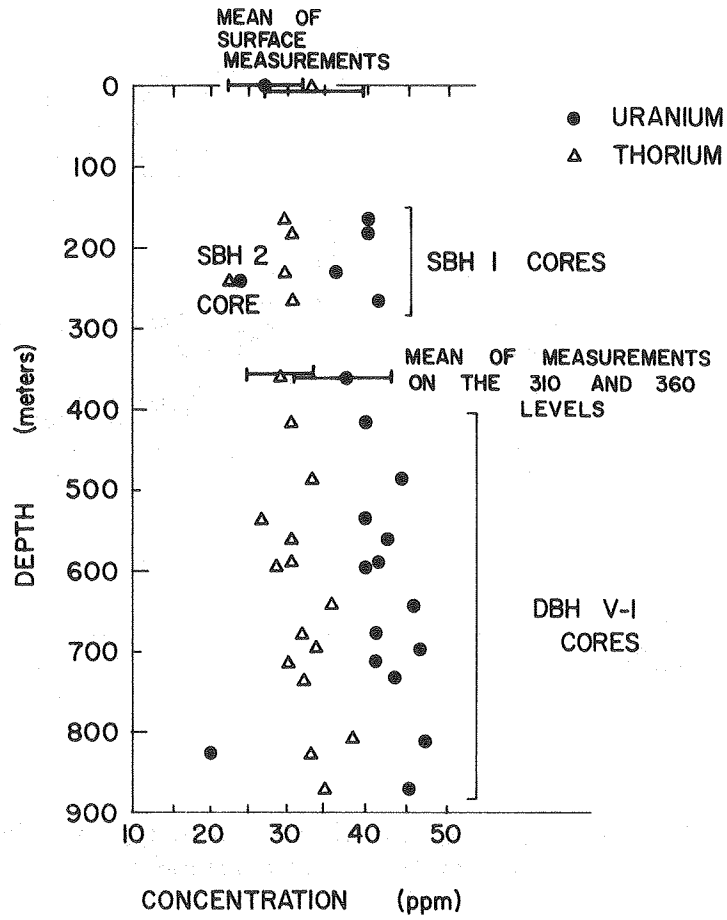
Fig. 21. Variation of uranium and thorium with depth in the Stripa quartz monzonite.

abundances in the same rock types underground. The underground/surface U concentration ratio, is 1.6 for the leptite, 1.4 for the quartz monzonite. A similar relationship holds for thorium in the leptite (1.7) but not in the quartz monzonite (0.9), nor for potassium in either the leptite or quartz monzonite. The Th/U ratio of the quartz monzonite is greater than 1 in the surface exposures and less than 1 in the subsurface.

It is well-documented in the literature that weathered exposures of crystalline rock are depleted in U compared with relatively unweathered exposures of the same rock. However, based on one author's (H.W.) experience, the glaciated surface outcrops of the quartz monzonite and leptite at Stripa are comparatively fresh, similar in some instances to glaciated exposures of granitic and metamorphic rock sampled at elevations of 1.5 to 2 km above sea level in the Sierra Nevada batholith, California. At these Sierran locations there were no appreciable differences between surface and subsurface samples in whole-rock uranium contents (Wollenberg and Smith, 1968).

An explanation for the differences between surface and subsurface U abundances at Stripa must therefore be sought elsewhere. Most U present at Stripa is found in one of two settings: in chloritic fracture zones, in which it is disseminated in relatively low concentrations; or in much higher concentrations in fine euhedral opaque grains (probably a uranium-thorium oxide mineral), commonly associated with fractures (see discussion in section 3.5). This situation may favor the removal of U from surface exposures by slightly acidic near-surface groundwater (Fritz et al. (1979) indicate that the pH of water from three wells in the quartz monzonite is 5.15, 6.6 and 7.6). In contrast, U in the Sierra Nevada batholithic rocks is

of considerably lower whole-rock abundance than at Stripa and is most strong-
ly associated with accessory minerals such as sphene, apatite, zircon, and
allanite. Therefore, U in the Sierra Nevada batholith is less accessible for
removal and transport by shallow ground water than at Stripa.

Detailed laboratory analyses of radioelements in cores from the bore-
holes drilled from the surface to the vicinity of the experimental area (SBH
1, 2, and 3) should help determine whether U increases gradationally with
depth or whether there is a sharp decrease in U near the surface. There is a
gradational increase in U and Th with depth below the 410 m level shown by the
laboratory gamma-spectrometric analyses of cores from the vertical borehole
DBH V-1 (Fig. 21). This apparent increase in radioelements with depth might
result from deeper portions of the vertical borehole having penetrated a zone
of the pluton where late-stage fluids containing oxyphile elements con-
centrated. The variation could also be influenced by the varying proximity
of the borehole to a diabase dike or dikes (see vertical cross section,
Fig. 5). The diabase is considerably lower in radioelement content than
the quartz monzonite.

3.6.3 Radioelements and the Age of Groundwater

Laboratory gamma-spectrometric analyses of U and Th contents in rock
were used to better define groundwater ages estimated by Fritz et al.
(1979), who employed the helium-4 method as well as other methods of age
dating. In estimating ages of groundwater from the M-3 hole, drilled
from the 330 m level in the experimental area, and from a zone in hole
DBH V-1 between depths of 376.5 and 471 m, Fritz et al. applied the
formula:

$$t = \frac{{}^4He \cdot n}{(U \cdot P_u + Th \cdot P_{th}) \xi} \qquad ,$$

where t is the apparent age, ^4He is the measured helium-4 concentration in cm^3/cm^3 of water, n is the estimated porosity of the rock, P_u and P_{th} are the helium production rates in cm^3 per g of radioelement per year, ξ is the rock density, and U and Th are concentrations in the rock in g/g. We applied the values of ^4He, n, P_u and P_{th} used by Fritz et al. and Th and U contents and rock density determined in this study to solve the above equation for t, the apparent age. The values used are listed in Table 10.

Solving for t yields an apparent age of the water in hole M-3 of 4.6×10^4 years, and 2×10^5 years for water in hole DBH V-1. These ages are compatible with the results of ^{14}C dating by Fritz et al. (1979), which indicated that waters discharging on the 330 m level and in borehole DBHV-1 were recharged more than to 20,000 years ago. The ^4He contents in the M3 and DBH V-1 holes differ by a factor of four, as do the calculated ages, because the whole-rock U and Th contents are fairly similar in the two water sampling locations. Greater U contents, such as those occasionally associated with chloritic fracture-filling material (Section 3.5) would result in proportionately younger apparent ages. The difference in ages indicates that the flow path of the deeper of the two groundwater systems was considerably longer than that of the shallower system; it also suggests that the bulk permeability of the rock decreases significantly with depth.

Table 10. Values used to calculate apparent ages of waters from Stripa boreholes.

Hole	^{4}He(cm^3/cm^3)	Mean U (g/g)	Mean Th (g/g)	n	ξ	P_u	P_{th}
M-3	3.5×10^{-4}	44×10^{-6}	30×10^{-6}	2×10^{-3}	$2.62 g/cm^3$	11×10^{-8}	3.1×10
DBH V-1	1.4×10^{-3}	38×10^{-6}	35×10^{-6}	2×10^{-3}	$2.62 g/cm^3$	11×10^{-8}	3.1×10

3.7 Radiogenic Heat Production and Heat Flow

The heat production, calculated from the radioelement contents of
the Stripa pluton, combined with the measured conductive heat flow, may
provide an estimate of the pluton's effective thickness, if a layered model
is considered. The heat production, A_0 (in μ W/m^3), was calculated from
the formula of Birch (1954):

$$A_0 = 10^{-5}\rho\ (9.69\ U + 2.65\ Th + 3.58\ K)$$

where ρ is the specific gravity of the rock, considered to be 2.62 in the
case of rocks of the Stripa region; U and Th are uranium and thorium concen-
trations in parts per million, and K is the potassium content in percent.

The radiogenic heat productions of the various rocks in the Stripa
region are listed in Table 9; the subsurface quartz monzonite averages 11.9 μ
Wm^{-3}. This compares with 2.8 μ Wm^{-3}, considered by Heier and Rogers
(1963) as the mean for granitic rocks, and $\sim$ 7 μ Wm^{-3} for other plutons in
the Stripa region and the Malingsbo granite. From Table 9 we see that the
radiogenic heat production of the Stripa quartz monzonite is 4 times that
of the neighboring leptite and 1.75 times the heat production of other
plutons in the region.

The conductive heat flow is the product of the thermal gradient and the
thermal conductivity of the rock within which the gradient was measured. The
gradient at Stripa was determined from a plot of the temperature measured by
geologists of the Chalmers Tekniska Högskola in hole DBH V-1 (Fig. 22).
The temperature versus depth curve is nearly linear from a depth of 160
m ($\sim$ 570 m below the surface) to the bottom of the hole, and gives a geo-
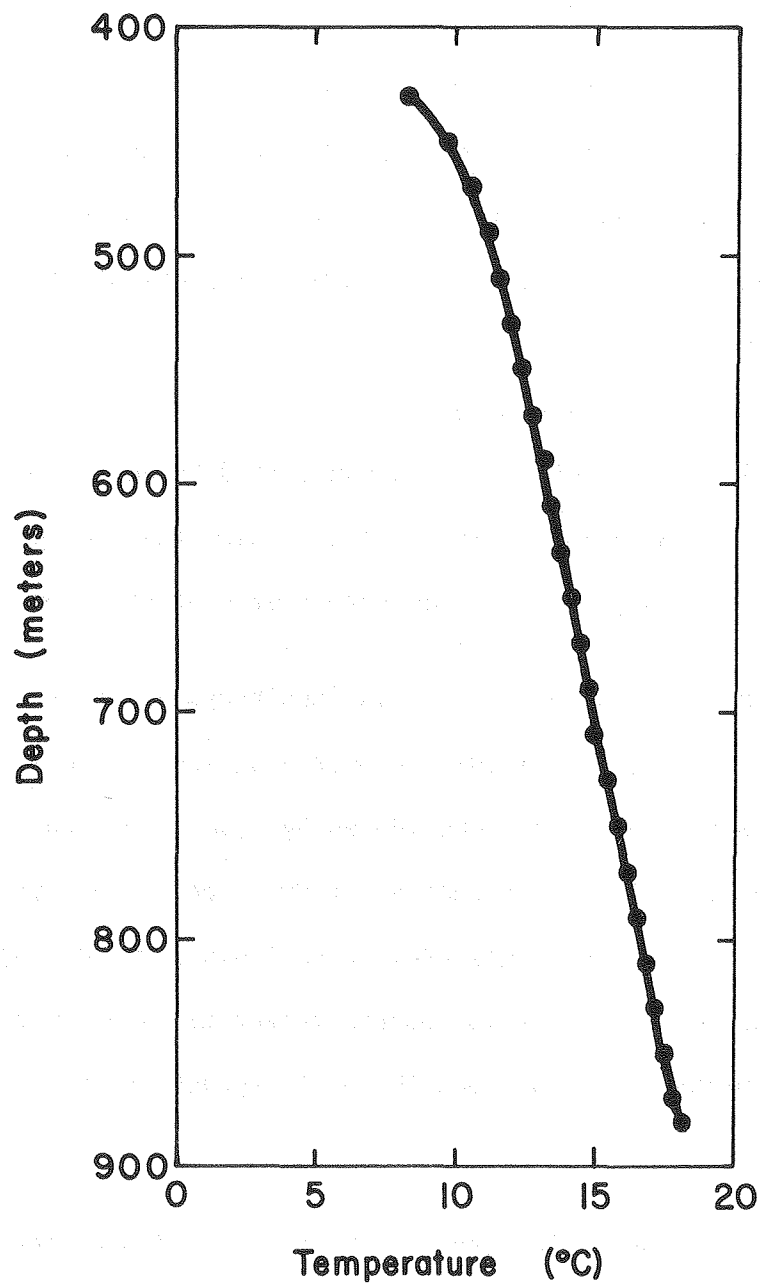
Fig. 22.   Temperature profile in borehole DBH V-1.

thermal gradient of 17.3°C/km.[1] The product of this gradient and the

thermal conductivity of 3.6 Wm^{-1} $°C^{-1}$ (Jeffry et al., 1979) is a heat flow

of 61.7 mWm^{-2}, a value close to that of the regional conductive heat flow

(uncorrected for glacial-climatic effects) of the south-central portion of

Sweden (Eriksson and Malmqvist, 1979).

A correction may be applied to the observed heat flow to account

for the glacial-climatic effects. Eriksson and Malmqvist (1979) point

out that because the average annual temperature increased in response

to the recession of the continental ice sheet in this region about 9500

years ago, the calculated correction to the observed geothermal gradient adds

3.2°C/km. This results in a corrected value of 20.5°C/km for Stripa, and

a resulting corrected heat flow of 73.8 mWm^{-2}.

Roy et al. (1968) developed the concept of the linear relationship

between conductive heat flow and radiogenic heat production. They proposed

that for Q, the observed heat flow,

$$Q = q^* + DA_0, \tag{1}$$

where q^* is the heat flow from below the upper portion of the earth's

crust within which most of the radioelements are concentrated, D is the

effective thickness of the radioactive layer, and A_0 is the radiogenic heat

production.

From heat flow and heat production measurements in central Sweden,

Landström et al. (1979), applying equation (1), estimated that D is 15.6

---

[1]There is a slight flow of water from DBH V-1, 120 to 240 liters per day; this
is considered to be too low to have an appreciable effect on the conductive
geothermal gradient measured in this 56 mm diameter hole (P. Nelson, private
communication, 1980).

km and $q* \simeq 25$ mWm^{-2}. Accepting these as the basic conditions for central Sweden, we can then estimate the effective thickness of the Stripa quartz monzonite, assuming a 2-layered case, by a modification of Eq. (1):

$$Q \simeq q* + D_1 A_1 + D_2 A_2, \qquad\qquad (2)$$

where D_1 and D_2 are the respective thicknesses (in km) of the quartz monzonite below 570 m depth and of rock of an underlying layer, and A_1 and A_2 their respective radiogenic heat productions in microwatts per cubic meter. Solving Eq. (2) using radiogenic heat productions of the quartz monzonite and metamorphic rocks (11.9 and 2.8 μ Wm^{-3} respectively), a corrected heat flow of 73.8 mWm^{-2}, a $q*$ of 25 mWm^{-2}, and a 15.6-km thick radioactive layer results in $D_1 = 0.75$ km, $D_2 = \sim 14.3$ km; this configuration suggests a total thickness of 1.3 km of Stripa quartz monzonite.

Alternatively, consider a layered intrusive configuration: quartz monzonite overlying rock with heat production of the other granitic rocks in the Stripa region (6.8 μWm^{-3}). If we assume that the effective thickness of the quartz monzonite is at least 1 km (drilling indicates that it is at least 900 m deep), Eq. (2) yields an effective thickness of 5.4 km for the underlying granitic rock. These alternative two-layer models are illustrated in Fig. 23.

However, a layered setting, where the Stripa quartz monzonite is the felsic outer zone of a large granitic pluton or a relatively thin plutonic veneer overlying a metamorphic basement, are two of several possible configurations: the Stripa pluton is just as likely to have intruded the metamorphic terrane as an unlayered stock or dike. These configurations would not lend themselves to the foregoing simplified layered model. Therefore, given current informa-
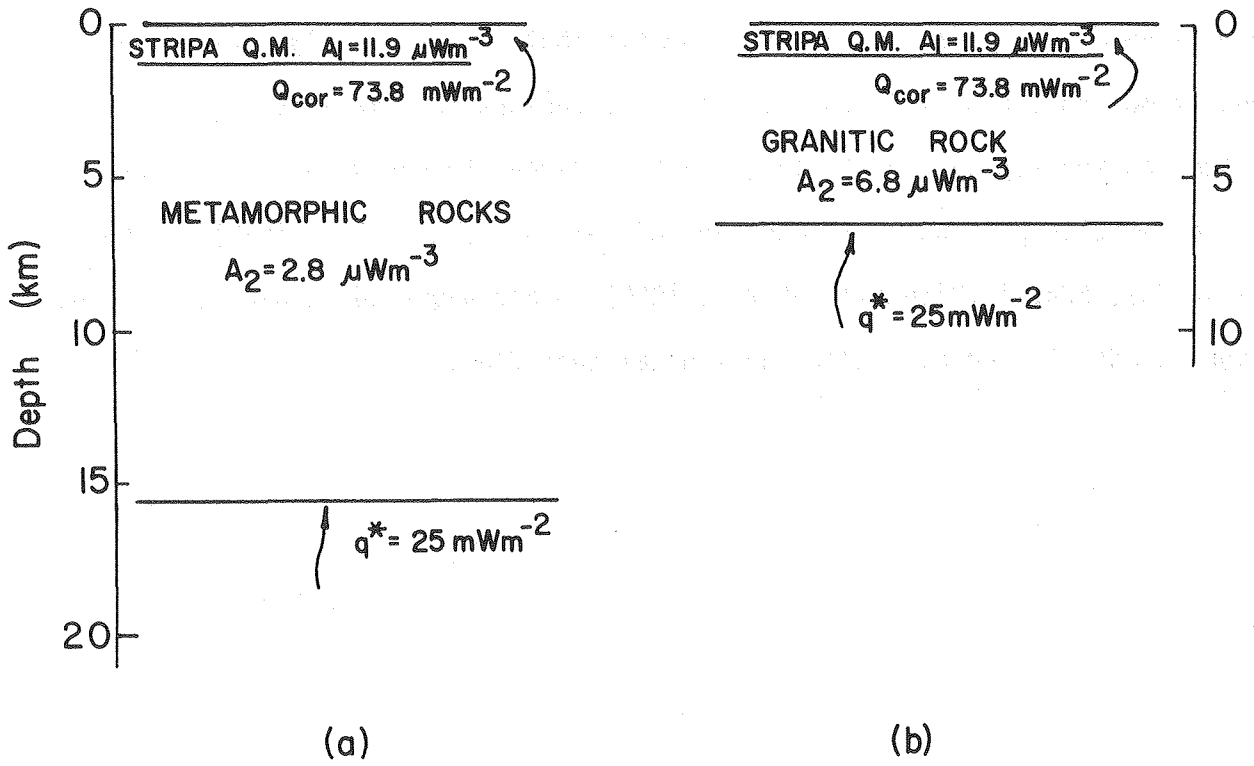
Fig. 23.   Layered models of a possible configuration of the
            Stripa pluton.

XBL 814-9182

tion, all we can state with assurance is that the high radiogenic heat production of the Stripa quartz monzonite, together with the regionally "normal" heat flow measured in the pluton, suggests that the relatively radioactive quartz monzonitic body is small; this body appears to have little if any effect on the regional heat flow. Similar circumstances were observed at the peralkalic plutons of Ilimaussaq, Greenland (Sass et al., 1972) and Pocos de Caldas, Brazil (Vitorello et al., 1980), where high radiogenic heat production is not matched by higher-than-normal heat flow.

4.0 SUMMARY

The Stripa quartz monzonite is ubiquitously fractured; fractures are spaced commonly as close as a few millimeters, and in places are less than a millimeter apart; their widths range from << 1 mm to several cm. Fracture-filling minerals were introduced in at least two stages, the earlier stage encompassing quartz, sericite, feldspar, epidote and chlorite, and the later stage dominated by carbonate minerals. Numerous fractures contain fillings of brecciated parent rock.

In contrast to other plutons in the Stripa region, where biotite and hornblende are prominent mafic minerals and accessory minerals are abundant, in the Stripa quartz monzonite muscovite is common, biotite has been altered to chlorite, hornblende is absent, and accessory minerals are scarce. Though the quartz monzonite and other plutons in the region have similar normative abundances of quartz, plagioclase and potassium feldspar, the quartz monzonite contains considerably less iron and magnesium. The apparent age of the quartz monzonite, determined by K-Ar dating of muscovite, is 1.69×10^9 years, an age close to those determined on biotites from granitic rock of the nearby Gusselby and Kloten massifs.

The quartz monzonite is considerably more radioactive than the other plutons near Stripa. Uranium and thorium are in roughly equal abundance (~ 30 ppm) in the quartz monzonite, while the Th/U ratio exceeds 2 in the other granitic rocks. Uranium is often found in euhedral opaque grains, in anhedral opaque grains of a distinctly different mineral, and disseminated in chloritic fracture-filling material.

The leptite is mineralogically similar to the Stripa quartz monzonite, though its radioelement content is considerably lower. The leptite is also strongly fractured, but epidote appears to be a more prominent fracture-filling mineral than in the quartz monzonite. The contact between the leptite and the quartz monzonite is generally sharp, but there is also some indication of a gradational contact between these two rock types.

Considerations of radiogenic heat production and heat flow suggest that the rock mass encompassed by the Stripa quartz monzonite is relatively small; though it contains high abundances of radioelements, these abundances have little effect on the regional heat flow. If the Stripa quartz monzonite is part of a layered geologic setting, it is probably not more than 1.5 km thick; if it is a stock, or dike, or felsic border phase, it would still be relatively small compared with the large granitic plutons exposed in the region.

ACKNOWLEDGMENTS

REFERENCES

Birch, F., 1954. "Heat from Radioactivity," in Nuclear Geology, H. Faul, ed., pp. 148-175, John Wiley, New York.

Deer, W.A., R.A. Howie, and J. Zussman, 1962. Rock Forming Minerals, Longmans, Green, & Co., Ltd., London.

Eriksson, K.G. and D. Malmqvist, 1979. "A Review of the Past and Present Investigations of Heat Flow in Sweden," in Terrestrial Heat Flow in Europe, V. Cermak and L. Ryback, eds., Springer Verlag.

Fritz, P., J.F. Barker, and J.E. Gale, 1979. Geochemistry and Isotope Hydrology of Groundwaters in the Stripa Granite: Results and Preliminary Interpretation. Lawrence Berkeley Laboratory report LBL-8285, SAC-12.

Geijer, P. and N.H. Magnusson, 1944. De Mellansvenska Järnmalmernas Geologi, Geological Survey of Sweden, Series Ca. nr. 35.

Geological Survey of Sweden, 1958. Bedrock Map of Sweden, Stockholm.

Geological Survey of Sweden, 1977. Jordartskartan, Lindesberg SV, S.G.U. Series Ae nr 30.

Geological Survey of Sweden, 1979. Geological Map of Lindesberg SW Quadrangle. Stockholm.

Hebert, A.J. and K. Street Jr., 1973. A Nondispersive Soft X-Ray Fluorescence Spectrometer for Quantitative Analysis of the Major Elements in Rocks and Minerals. Lawrence Berkeley Laboratory report LBL-1616.

Heier, K.S. and J.J.W. Rogers, 1963. "Radiometric Determinations of Thorium, Uranium and Potassium in Basalts and in Two Magmatic Differentiation Series" Geochim. Cosmochim. Acta, vol. 27, pp. 137-154.

Jeffry, J.A., T. Chan, N.G.W. Cook, and P.A. Witherspoon, 1979. Determination of In-Situ Thermal Properties of Stripa Granite from Temperature Measurements in the Full-Scale Heater Experiments: Method and Preliminary Results. Lawrence Berkeley Laboratory report LBL-8423, SAC-24.

Koark, H.J. and I. Lundström, 1979. Berggrundskartan, Lindesberg, S.V., Geological Survey of Sweden, S.G.U. Series AF nr 126.

Landström, O., G. Lind, S-Å Larson, and D. Malmqvist, 1979. Värmeflöde i Berg, publ. B137. Chalmers University of Technology, Department of Geology (in Swedish).

Magnusson, E., 1978. Description of the Quaternary Map, Lindesberg, S.V., Geological Survey of Sweden, S.G.U. Ser. Ae, no. 30, Stockholm.

Nelson, P., R. Rachiele, and A. Smith, 1980. The Effect of Randon Transport in Groundwater upon Gamma-Ray Borehole Logs. Lawrence Berkeley Laboratory report LBL-11180, SAC-30.

Olkiewicz, A., J.E. Gale, R. Thorpe, and B. Paulsson, 1979. Geology and Fracture System at Stripa. Lawrence Berkeley Laboratory report LBL-8907, SAC-21.

Olkiewicz, A., K. Hansson, K-E Almen, and G. Gidlund, G., 1978. Geologisk och hydrogeologisk grunddokumentation av Stripa Forsoks station. Karnbranslesakerhet Teknisk Rapport 63.

Roy, R.F., D.D. Blackwell, and F. Birch, 1968. "Heat Generation of Plutonic Rocks and Continental Heat-Flow Provinces," Earth Planet. Sci. Lett., vol. 5, no. 1, pp. 1-12.

Sass, J.H., B.L. Nielsen, H.A. Wollenberg, H.A. and R.J. Munroe, R.J. 1972 "Heat flow and Surface Radioactivity at Two Sites in South Greenland", Jour. Geophys. Res., vol. 77, pp. 6435-6444.

Ihorpe, R., D.J. Watkins, W.E. Ralph, R. Hsu, and S. Flexser, 1980. Strength and Permeability Tests on Ultra-large Stripa Granite Core. Lawrence Berkeley Laboratory report LBL-11203, SAC-31.

Vitorello, E., V.M. Hamza, and H.N. Pollack, H.N. 1980. "Terrestrial Heat Flow in the Brazilian Highlands," Jour. Geophys. Res., vol. 87, pp. 3778-3788.

Welin, E., 1964, "Pitchblende-Bearing Vein Fillings in the Stripa and Blanka Iron Ores," Geologiska Föreningens i Stockholm Förhandlingar, vol. 86, pp. 257-270.

Welin, E., A-M Kahr, and P.H. Lundegardh, 1980. "Rb-Sr Isotope Systematics at Amphibole Facies Conditions, Uppsala Region, Eastern Sweden," Precambrian Research, vol. 13, pp. 87 - 101.

Wollenberg, H.A. and A.R. Smith, 1968. "Radiogeologic Studies in the Central part of the Sierra Nevada Batholith," Jour. Geophys. Res., vol. 73, no. 4, pp. 1481-1495.

Wollenberg, H.A. 1972. "Fission Track Radiography of Uranium and Thorium in Radioactive Minerals, "in Geochemical Exploration, 1972. Institute of Mining and Metullurgy, London, pp. 347-358.

APPENDIX A: DESCRIPTION OF THIN SECTIONS

Thin sections cut both from core samples and hand samples are described, with particular emphasis on fracture-fill mineralogy and texture. The non-fractured matrices of the samples from Stripa are not generally described in detail except where they differ significantly from typical textures summarized earlier in the text.

1. Core Samples

These samples, designated by an S prefix, were cut from cores from the two surface boreholes SBH-1 and SBH-2, and from the deep borehole DBH-V1 (see Fig. 2). They are indexed according to their positions on the respective cores. The more fractured or brecciated portions of the cores were preferentially sampled for thin sections, but relatively unfractured samples were also taken.

S-1 (SBH-1, 51.63 m)

Light reddish granitic matrix cut by network of fine fractures grading to microbreccia. Fracture-filling materials are chlorite, quartz, sericite, carbonate, and, possibly, lesser altered epidote; carbonate is the major filling in coarse fractures and breccias.

S-2 (SBH-1, 52.69 m)

Foliated leptite matrix containing quartz porphyroblasts, cut with a network of narrow light veinlets. Veinlets (up to ~ 0.3 mm wide) consist of very finely intergrown quartz, feldspars, and lesser chlorite and sericite, and locally include near-opaque altered epidote(?). Matrix is also cut by finer veinlets (up to 0.1 mm wide) of quartz and of carbonate.

S-3   (SBH-1, 77.81 m)

Foliated, porphyroblastic leptite matrix, relatively poor in chlorite. It is cut by numerous prominent discontinuous fractures, ~ 1 mm wide, which are filled with a light-colored intergrowth of coarse-grained epidote, carbonate, and fluorite, and include fine fragments broken from the leptite matrix. Epidote also occurs in scattered patches in the matrix, where it is commonly altered and near-opaque.

S-4   (SBH-1, 109.92 m)

Strongly foliated, non-porphyroblastic dark leptite matrix cut by fractures similar to those of S-3, and filled with both coarse and fine epidote, quartz, carbonate, and fine sericite. Epidote occurs also in isolated patches in the matrix.

S-5   (SBH-1, 185.17 m)

Light reddish leptite matrix, resembling pegmatite in hand specimen, cut by thick light-green fracture zone. Matrix is composed of even, fine-grained mosaic of quartz and microcline, with sparse elongate grains of fine chlorite and epidote defining a foliation. Muscovite is absent, plagioclase rare. Fracture zone is up to 1 cm wide, filled with coarse epidote; it grades to microbreccia composed of angular fragments broken from the leptite, and interstitial epidote. In addition, narrower fractures (ranging from 1 mm wide down to fine strings) with epidote or carbonate-quartz fillings, are abundant in the matrix. The carbonate-quartz veins are subsequent to the epidote veins, as epidote veins (as well as the large fracture zone) are commonly displaced across them.

S-6 (SBH-1, 207.75 m)

Fractured and brecciated leptite. Light green breccia ~ 1 cm wide is bordered by darker breccia, and between these is a fluorite-filled fracture up to 2 mm wide. The darker breccia is composed of fragments of leptite with interstitial epidote, chlorite, sericite, and fluorite. The lighter breccia contains a similar mineralogy, but with much coarser interstitial fillings of fluorite with acicular carbonate and quartz euhedra. The original texture of the matrix is largely obscured by brecciation, but it appears to be poorly foliated porphyroblastic leptite.

S-7 (SBH-1, 232.85 m)

Reddish granitic matrix, highly fractured and brecciated. Fractures are filled with chlorite, sericite, and lesser quartz and carbonate. Breccia zones contain a similar mineralogy dominated by carbonate, and brecciated feldspar grains are generally reddened by diffused hematite alteration, or are totally altered to sericite. Matrix contains traces of garnet.

S-8 (SBH-1, 278.45 m)

Dark green, fine-grained amphibolite, cut by prominent light fractures. Amphibole is pale green prismatic actinolite, intergrown with quartz and opaque grains, and including sericite (possible altered feldspar), chlorite, and carbonate in isolated patches and as fillings of fine fractures. The prominent fractures (up to 3 mm wide) are filled with carbonate, bordered by opaque material (hematite?), and include lenses rich in chlorite and quartz.

S-9 (SBH-1, 278.55 m)

Fracture zone, 5-10 cm wide, cutting amphibolite. Fracture filling consists of narrow white, dark green, light green and red lenses of carbonate,

quartz, chlorite, sericite, epidote, and hematite. Lenses may be either monomineralic (particularly carbonate, sutured quartz, or chlorite) or fine intergrowths of several minerals. Some include brecciated fragments of either leptite or fine-grained granitic rock. Where sequential relations can be interpreted, calcite appears to be the latest filling.

S-10 (SBH-1, 280.13 m)

Dark green fracture zone in contact with red granitic rock. Fracture zone contains brecciated granitic rock with some well-rounded fragments, and is strongly foliated due to parallel veins and lenses of chlorite, carbonate, altered epidote, and opaque material. The granitic rock is composed mainly of quartz and plagioclase, with little or no microcline, and grades locally into a microbreccia with interstitial sericite. Fine fractures filled with quartz and opaques, carbonate, or sericite-chlorite-altered epidote cut this granitic matrix. The contact between granitic rock and fracture zone is parallel to the foliation of the fracture zone and is marked by a 1-mm-wide band of fine-grained granitic rock also foliated parallel to the contact. This rock is composed of quartz and feldspars with elongate chlorite grains, and is not distinguishable from leptite.

S-11 (SBH-1 291.87 m)

Light reddish granitic matrix cut by breccia zone ~ 0.5 cm wide. Interstices of breccia are filled with chlorite and epidote, and included feldspar grains show hematite alteration. Smaller fractures run sub-parallel and intersect breccia zone, and are filled with epidote, quartz, and chlorite. Coarse epidote prisms (up to 0.5 mm) present in some fractures are often fresh, while finer-grained epidote is usually altered and near-opaque.

S-12 (SBH-1 320.65 m)

    Reddish granitic matrix, relatively unfractured. Chloritized biotites have abundant pleochroic halos, some with distinct grains (zircon?) within. Fractures include a 0.1 mm-wide continuous carbonate vein, with lesser quartz and fluorite, and finer discontinuous sericite fractures.

S-13 (SBH-1 371.47 m)

    Grey granitic matrix cut by microbreccia composed of broken fragments of granitic parent rock. Interstices of breccia are filled with chlorite, carbonate, sericite, and occasional pyrite. Light green continuous fracture ($\leq$ 0.2 mm wide) cuts through breccia zone, and is filled with nearly opaque altered fine epidote (?) bordered by chlorite and sericite. Matrix contains traces of garnet.

S-14 (SBH-2 6.79 m)

    Medium- to coarse-grained amphibolite composed mainly of blue-green amphibole and strongly altered plagioclase. Fine fractures (and some coarser, up to 0.5 mm wide) filled with carbonate or epidote are abundant. Plagioclase is altered to fine sericite and coarse epidote or clinozoisite; a vein of plagioclase 1-3 mm wide also cuts the rock, and includes an isotropic mineral (garnet?). Opaque grains are common, and some are altered epidote. Accessory apatite is also present.

S-15 (SBH-2, 14.62 m)

    Strongly foliated fine- to medium-grained amphibolite. Foliation is due to parallel alignment of blue-green amphiboles, and also to parallel lenses alternately rich in plagioclase, quartz, or chlorite, which are intergrown with amphibole. Plagioclase is very altered to sericite. Chlor-

ite grains contain abundant pleochroic halos surrounding fine high relief grains (zircon?); chlorite likely formed by alteration of biotite, as partly chloritized biotite grains are intergrown with chlorite. Quartz-rich lenses have a sutured texture, contain amphiboles, and texturally resemble leptite. Carbonate occurs as fine discontinuous stringers, and epidote occurs as tiny interstitial grains.

S-16 (SBH-2, 16.19 m)

Medium-grained dark-green amphibolite cut by light green, mainly epidote-filled fractures. Blue-green amphiboles are intergrown with dusty quartz and lesser epidote and near-opaque grains (altered epidote?). Fractures are commonly 1-3 mm wide, filled with coarse-grained epidote, with stringers of carbonate and quartz within and parallel to the fractures.

S-17 (SBH-2, 36.01 m)

Fractured light reddish granitic rock in contact with foliated leptite. Prominent fracture cutting granitic rock is 1-2 mm wide, filled with quartz, epidote and lesser sericite, and associated with anhedral U-rich opaque grains up to 0.5 mm in diameter. Fine stringers of carbonate and sericite, offshoots from the main fracture, cut the granitic rock, and include similar U-rich grains. The granitic rock is also cut by a clayey quartz-chlorite-filled fracture 1-2 mm wide. The leptite is composed of intergrown quartz, feldspars and abundant muscovite laths, contains quartz porphyroblasts, and is cut by a 0.5 mm wide chlorite-filled fracture. The contact between leptite and granitic rock is sharp, and is otherwise marked only by sparse epidote grains.

S-18 (SBH-2, 50.14 m)

Leptite in contact with pale reddish aplitic granitic rock. The leptite is porphyroblastic, moderately foliated, and similar to the leptite of sample S-17. The granitic rock is composed of quartz and myrmekitic plagioclase, with coarse laths of muscovite in preferred orientation perpendicular to the contact with leptite. Both granitic rock and leptite are cut by prominent light green fractures (up to 0.5 mm wide) filled with altered, near-opaque epidote and by finer quartz-filled fractures. The contact is marked by an abundance of sericite and is in part coincident with an epidote-filled fracture.

S-19 (SBH-2, 50.62 m)

Fine-grained, foliated, porphyroblastic leptite with prominent light-green fractures up to 3 mm wide. The fractures are filled with coarse-grained epidote with some intergrown quartz. Quartz stringers run within, and parallel to, the fractures. Fine quartz veins are also abundant else-where in the leptite, and the coarse epidote veins are offset by them.

S-20 (SBH-2, 124.33 m)

Light reddish granitic matrix cut by several types of fractures. A set of black sub-parallel fractures, filled mainly with chlorite and grading locally into microbreccia ($\leq$ 1 mm wide), is most prominent. It is cross-cut by a light green fracture (0.5 mm wide) filled with epidote, quartz, and minor fluorite, and by a fine veinlet of carbonate, sericite, and chlorite (<0.05 mm wide).

S-21 (SBH-2, 178.01 m)

Pyrite-rich fracture zone in reddish granitic rock. Coarse-grained pyrite, with chlorite, sericite, epidote, and near-opaque altered epidote, are densely intergrown several centimeters wide in the fracture zone. The granitic rock is very rich in microcline and quartz and poor in plagioclase; coarse muscovite crystals are abundant and commonly kinked. The granitic rock is pervasively fractured to yield an angular breccia, with coarse interstices filled with a mineral assemblage similar to that in the fracture zone, and finer interstices filled with sericite, chlorite, or fluorite.

S-22 (SBH-2, 208.54 m)

Reddish granitic matrix cut by sets of sub-parallel black fractures grading to microbreccia. Fracture fill is dominated by opaque material, mostly hematite, which obscures much of the other fracture-filling material consisting of chlorite, quartz, and epidote (largely altered).

S-23 (SBH-2, 213.55 m)

Brecciated reddish granitic matrix. Granitic fragments grade completely from millimeters to <0.1 mm in size, and are commonly rounded. Interstices of breccia are filled predominantly with fluorite and also contain chlorite and hematite and other opaque material. Fracture (<0.5 mm wide) cutting breccia is filled with carbonate needles in fluorite, with lesser altered epidote(?).

S-24 (SBH-2, 227.05 m)

Aplitic dike or inclusion in contact with highly fractured reddish granitic rock. Aplite portion is composed mainly of sutured quartz grains, with lenses or veins of muscovite and lesser opaque grains and chlorite.

Granitic portion is cut by fractures filled with sericite, chlorite, and opaque grains. Contact is a fracture zone filled with opaque grains, muscovite, chlorite, and accessory garnet. Opaque mineral is at least in part hematite; opaque alteration is also common in muscovite cleavage planes.

S-25 (SBH-2, 251.67 m)

Grey granitic matrix, moderately fractured. Fractures are generally <0.2 mm wide, and are filled with epidote (largely altered), sericite, and chlorite. Matrix contains scattered opaque grains (pyrite?) and traces of garnet.

S-26 (SBH-2, 252.02 m)

Grey granitic matrix, moderately fractured. Fractures range in width up to 1 mm, and are filled with quartz, epidote (largely altered), chlorite, and sericite. They are also filled locally with microbreccia.

S-27 (SBH-2, 289.95 m)

Pegmatite in contact with grey granitic rock. Contact surface is a fracture 0.5 - 1.0 mm wide filled with chlorite, pyrite, muscovite and traces of sphene or epidote. Pegmatite is rich in microcline, and contains aggregates of coarse muscovite grains with intergrown pyrite, and accessory garnet; it is cut with chlorite-pyrite-filled fractures, and fine quartz veins. Granitic rock in contact with pegmatite contains highly sericitized plagioclase, and is cut by fine chlorite-filled fractures.

S-28 (SBH-2, 324.57 m)

Grey to light pink fractured granitic matrix with accessory grains of pyrite and garnet. Most prominent fracture zone is 1-2 mm wide, filled with

a central band of chlorite bordered by intergrown pyrite, sericite, and chlorite, and containing local concentrations of garnet. Widest portions of this fracture zone contain brecciated fragments of parent rock. Other fractures are finer (generally ~ 0.1 mm wide), filled with either sericite and chlorite, or fluorite, carbonate, and chlorite.

S-29 (SBH-2, 340.31 m)

Grey granitic matrix, fractured and brecciated. Several major fractures, up to 1 mm wide, are filled with coarse crystals of quartz and purple fluorite. Most of sample is cut with a network of fine sericite-chlorite-filled fractures which commonly grade to breccia composed of angular fragments of parent rock and some fluorite grains.

S-30 (SBH-2, 340.73 m)

Granitic matrix, thoroughly brecciated to angular fragments and very finely comminuted material. Interstices of breccia filled with chlorite-sericite intergrowth, with associated opaque material (altered epidote?). Breccia is cut by 0.5 mm wide fracture filled with purple fluorite, quartz, and accessory garnet; fluorite grains are included locally as fragments in breccia, indicating that brecciation was in part subsequent to fluorite veining.

S-31 (SBH-2, 350.43 m)

Light reddish granitic matrix, cut by several zones of parallel fractures, 1-2 mm wide, which grade locally to microbreccia. These fractures are dark green and filled with near-opaque intergrowths of altered epidote and chlorite. Very fine fractures also parallel the main fractures, and are filled with grains of quartz and feldspar and traces of fluorite.

S-32 (SBH-2, 358.50 m)

Moderately fractured reddish granitic matrix intersected by densely

fractured and brecciated zone. Less fractured portion is cut by fine chlor-

ite-sericite veins and fine carbonate veins. Densely fractured zone contains

fractures filled with intergrowths of coarse-grained chlorite, epidote, and

carbonate, as well as irregular patches of muscovite, chlorite, epidote, and

opaque grains (pyrite?). Breccia consists of angular and rounded fragments

of granitic rock, with interstitial carbonate, chlorite, and epidote.

Cutting the breccia is a fracture 3-5 mm wide, strongly foliated parallel to

the fracture surface, filled with dense chlorite containing lenses of epi-

dote, carbonate and mylonitic breccia derived from the granitic parent

rock.

S-33 (SBH-2, 358.73 m)

Dike in contact with granitic breccia, with contact zone between.

The granitic breccia is continuous in core sample with S-32; its texture has

progressed, however, toward that of mylonite gneiss. It is strongly foliated

parallel to the leptite contact, with the foliation defined by lenses filled

with a mosaic of finely recrystallized quartz, and by stringers of sericite

and chlorite. Broken and occasionally rounded fragments of granitic rock

occur as augen within the mylonitic breccia.

The contact consists of a 5-mm-wide, strongly foliated zone resembling

the dense fracture zone in S-32, and consisting of alternating convoluted

layers of carbonate, chlorite, mylonite, epidote, and pyrite. Narrow veins

of carbonate, chlorite, and epidote which cut the mylonite breccia are

truncated by this contact zone. The contact with the dike is sharp, and fine

fractures nearly perpendicular to the contact, filled with carbonate and chlorite, cut the dike.

The dike is composed of a dark, fine-grained rock which, although logged in drill cores as a leptite, is not similar to the leptites studied here. Its texture is strongly porphyritic, resembling that of a volcanic rock (on the evidence from core samples alone, the possibility that it may be a faulted slice of a volcanic rock cannot be discounted), with plagioclase laths, generally elongate parallel to the contact, set in a very fine grained groundmass. Plagioclase is strongly altered to sericite and chlorite, relict pyroxene(?) grains are altered entirely to chlorite, and the groundmass is coated with a clay veneer.

S-34 (DBH V-1, 4.55 m)

Grey granitic matrix, relatively unfractured, with occasional discontinuous fractures filled with sericite and chlorite. One prominent fracture, 0.2-0.5 mm wide, cuts the matrix, and is filled with chlorite, carbonate, sericite, and pyrite, with lesser quartz and traces of epidote.

S-35 (DBH V-1, 16.07 m)

Grey to light pink granitic matrix, largely brecciated. Interstices of breccia are mainly chloritic, with lesser carbonate. Fractures filled with carbonate and quartz cut the breccia, and most are discontinuous.

S-36 (DBH V-1, 16.12 m)

Granitic breccia similar to S-35. Carbonate occurs as a common fracture filling, with quartz. It also occurs as isolated patches within the breccia, where it is sometimes associated with chlorite, opaques, or traces of epidote.

S-37 (DBH V-1, 73.30 m)

Grey granitic matrix, cut by numerous fractures. Most fractures are light green, <0.5 mm wide, and filled with epidote, sericite, and quartz, with local accumulations of pyrite euhedra. These fractures are sub-parallel; locally they converge and may be filled with microbreccia. Other fractures are oriented near-perpendicular to this set (without apparent offset), and are filled with chlorite, sericite, and, locally, pyrite.

S-38 (DBH V-1, 125.20 m)

Grey granitic matrix, relatively unfractured, containing traces of garnet. Some very fine fractures, filled with sericite and chlorite, are present; these are of small extent and usually adjacent to primary mica grains.

S-39 (DBH V-1, 168.97 m)

Light grey garnetiferous granitic matrix (aplitic), lacking primary biotite. Garnets range up to 1 mm in diameter, are pink and often rounded, and are commonly fractured and partly altered to chlorite and sericite. The matrix is cut with fractures up to 0.2 mm wide filled in part with chlorite, quartz, and lesser carbonate and fluorite, and in part with microbreccia.

S-40 (DBH V-1, 264.87 m)

Grey granitic matrix, moderately fractured. Two narrow (0.1 mm wide), convergent light green fractures cut the matrix, and are filled with a near-opaque, fine-grained intergrowth of altered epidote, sericite, and chlorite. Where they converge, they form one fracture, 3 mm wide, filled with microbreccia with interstitial chlorite. The matrix is otherwise cut only by narrow discontinuous chlorite- and sericite-filled fractures.

S-41 (DBH V-1, 299.39 m)

Brecciated grey granitic matrix. Fragments in breccia include finely comminuted material and sub-rounded clasts, up to 1 cm in diameter, of relatively unfractured granitic rock. Interstices of breccia are filled with chlorite and lesser hematite. Breccia is cut by narrow light green epidote-filled fractures, and by a thicker fracture (>2 mm) filled with coarse epidote and finely intergrown sericite and chlorite.

S-42 (DBH V-1, 313.14 m)

Red granitic breccia, cut by light green mylonitic zones. Breccia consists of finely ground granitic rock, probably largely recrystallized, with dispersed sericite, chlorite, and hematite, and includes granitic fragments, both rounded and angular, up to 0.5 mm in diameter. Narrow fractures filled with quartz and chlorite cut the breccia. Mylonitic zones are characterized by sub-parallel alignment of convoluted lenses containing opaque material (partly hematite, partly altered epidote?), fine-grained quartz, or chlorite-sericite intergrowths, all rich in clay and including fine granitic breccia. Carbonate is nearly or entirely absent.

S-43 (DBH V-1, 349.50 m)

Fine-grained grey granitic matrix, with isolated intergranular patches of epidote up to 1 mm in diameter. The matrix also contains very abundant fine intergrowths of quartz and feldspars and less commonly sericite along grain boundaries, and lacks primary biotite. The matrix is cut by one major fracture, 3-4 mm wide, filled with finely intergrown chlorite and quartz, and including fine granitic microbreccia, and lenses rich in epidote and clay. Carbonate occurs in tiny stringers running parallel to this main fracture,

and in occasional intergranular patches like those filled with epidote.

S-44 (DBH V-1, 392.71 m)

Grey granitic rock in contact with dark grey foliated granitic rock resembling leptite. Non-foliated portion is typical Stripa quartz monzonite, composed of sutured quartz, plagioclase (sericitic), microcline, and musco- vite and chloritized biotite which are largely interstitial. It is also characterized by a very uneven grain-size distribution. The foliated gran- itic rock contains a similar mineralogy, but has a much more even grain-size distribution, and a foliation defined by parallel orientation of abundant chlorite grains. Small high-relief grains (zircon or allanite?) are common in the chlorite. Both foliated and non-foliated portions are cut by fine fractures filled with chlorite and sericite and in some cases epidote. The contact between the two granitic rocks is not as pronounced in thin section as it is in hand specimen, and is marked only by thin veinlets of chlorite rich in the high-relief mineral.

S-45 (DBH V-1, 392.86 m)

Reddish granitic rock in contact with dark grey foliated granitic rock, very similar to S-44. The foliated, leptite-like portion contains coarse-grained poikilitic microcline, and relatively little quartz. The contact is a plane of abrupt textural transition, but is not otherwise marked, as with a fracture. Prominent light green narrow fractures (<0.5 mm wide) cut both portions of the thin section at high angles to the contact, and are filled with epidote, quartz, and traces of carbonate.

S-46 (DBH V-1, 406.71 m)

Grey fractured granitic matrix in contact with breccia. Breccia
is composed of granitic fragments commonly up to 1 mm in diameter, generally
angular, with interstices filled with finer fragments, chlorite, and patches
of epidote. The non-brecciated granitic rock is cut with fine fractures
filled with near-opaque altered epidote and/or hematite, and microbreccia.

S-47 (DBH V-1, 407.97 m)

Complexly fractured granitic matrix. Two prominent sub-parallel
fracture zones, up to 3-4 mm wide, are filled mainly with carbonate, and
contain lenses of microbreccia, chlorite, altered epidote, and opaque mater-
ial. Another coarse fracture, 2-3 mm wide, runs between them, and is light
green in color and filled mainly with near-opaque altered epidote. In
addition, fine fractures filled with quartz, chlorite, epidote, opaques, and
lesser carbonate cut the matrix at varied orientations. The matrix itself
shows extensive alteration of primary muscovite to chlorite and opaques, and
contains traces of garnet.

S-48 (DBH V-1, 414.61 m)

Brecciated red granitic matrix, cut by thick light green fracture
zone. Brecciation is due to a network of irregular fine fractures which
completely pervade the rock, and which are filled with sericite, chlorite, or
altered epidote, and locally with quartz. Fracture zone is ≥ 1 cm wide, and
is filled with a near-opaque dense intergrowth of altered epidote, chlorite,
and clay, with included granitic fragments and occasional carbonate patches.

S-49 (DBH V-1, 464.74 m)

Grey granitic matrix, moderately fractured. Prominent dark fracture, ~ 0.5 mm wide, is filled largely with altered epidote and broken granitic parent rock, and has very thin borders of sericite. Finer fractures filled with carbonate and quartz cut the matrix parallel to the main fracture. Matrix contains traces of garnet.

2. Hand Samples from Stripa and Vicinity

These samples are designated by an ST prefix. For sampling localities see Figs. 2, 3, and 4.

ST-1

Grey strongly foliated leptite, composed of finely intergrown quartz, lesser plagioclase and microcline, and abundant elongate parallel muscovite grains. Quartz porphyroblasts are abundant. Plagioclase is largely altered to sericite. Muscovite is often intergrown with chlorite and, to a lesser extent, with epidote. Fine fractures are filled with sericite and chlorite, and often with hematite as well.

ST-3

Reddish granitic matrix, relatively unfractured. Only fine, quartz-filled fractures are present, as well as discontinuous cracks filled with chlorite, sericite and some dispersed hematite.

ST-9

Light reddish granitic matrix, cut by a dark fracture ($\leq$ 0.5 mm wide) filled with chlorite, sericite, and locally with microbreccia. The matrix contains abundunant cracks filled with chlorite, sericite, or finely inter-

grown quartz and feldspars, and contains traces of garnet.

ST-12

Light reddish granitic matrix, similar to ST-3, with occasional stringers of carbonate (< 0.03 mm wide).

ST-18a

Light grey granitic matrix, relatively unfractured and similar to ST-3, but with extensive sericitic alteration of plagioclase. Contains accessory pyrite.

ST-19

Grey granitic matrix, similar to ST-18a.

ST-21

Light reddish granitic matrix, similar to ST-12.

ST-27

Dark grey strongly foliated leptite, texturally similar to ST-1, but slightly coarser-grained and lacking porphyroblasts. Feldspars are largely absent, although small areas occur which are rich in plagioclase to the exclusion of quartz and in which the foliation is less well defined. Biotite, partly replaced by chlorite, is very abundant, and, along with less abundant muscovite, defines the foliation. Biotite grains contain fine elongate birefringent grains (zircon?).

ST-32

Fractured, light grey leptite, composed of intergrown quartz, plagio-
clase (very altered), and microcline, with lesser muscovite and chlorite.
Foliation is not strongly pronounced. Most prominent fractures (up to 1 mm
wide) are filled with quartz, and finer fractures are generally filled with
very fine intergrowths of chlorite, quartz, and feldspars, locally resembling
microbreccia.

ST-35

Black, fine-grained diabase composed mainly of intergrown plagio-
clase, pyroxene, and magnetite. Pyroxene is largely altered to chlorite,
sericite, and needle-like growths of an opaque mineral. Plagioclase is
partly altered to sericite. Interstices between grains are generally filled
with fine-grained alteration products, including clay, chlorite, and possibly
epidote. One prominent fracture, 0.5 mm wide, cuts the diabase, and is
filled with chlorite, carbonate, and lesser magnetite.

3. Hand Samples from Other Granitic Massifs Near Stripa

These samples are from other granitic massifs near Stripa. See Appendix
C for sources and locations. Fractures are less abundant and pronounced in
these samples than in the Stripa rocks, and thin section descriptions are
thus concerned mainly with the matrix.

Gusselby Massif

J74-1

Red, medium-grained granitic rock. Microcline is abundant and coarse-
grained, with some sericite alteration. Biotite is relatively sparse and is
partly altered to chlorite (preferentially along cleavage planes), partly

fresh, and often contains dense pleochroic halos, with discrete, near-isotropic grains within. Muscovite is present but not abundant. Fine zircon(?) grains are scattered among intergrowths of biotite, muscovite, chlorite, and opaque grains (pyrite?). Opaque grains and apatite occur elsewhere as accessory minerals. Sericite, chlorite, and intergrowths of quartz and feldspars fill fine discontinuous cracks within grains or along grain boundaries, resembling the Stripa quartz monzonite in this respect.

J75-1

Red granitic rock, similar to J74-1, with lesser microcline and more abundant, relatively fresh biotite. Also contains carbonate locally inter-grown with micas, chlorite, and opaque grains, and has traces of fluorite.

L79-1

Light reddish granitic rock similar to J74-1 and J75-1, but more exten-sively altered. Biotite is thoroughly chloritized, and plagioclase is very clouded with diffused clay alteration and cut with cracks filled with chlorite and sericite. Muscovite is nearly absent.

Dammsjön Massif

J75-4

Coarse-grained, light reddish granitic rock, friable due to network of fine, unfilled cracks. Plagioclase is very cloudy, commonly with sericite or chlorite alteration, occasionally with epidote, opaque (hematite?), or carbonate alteration. Microcline is particularly coarse-grained and often poikilitic. Biotite is very abundant, coarse-grained, and fresh, with only minor chlorite alteration. Primary muscovite is absent. Green hornblende is commonly intergrown with biotite, as are small grains of sphene and possibly

zircon. Apatite is a common accessory mineral; fluorite is present in trace amounts.

J75-7

Coarse-grained grey granitic rock, very similar to J75-4, but somewhat less cracked and friable. Biotite is somewhat more chloritized; hornblende is less abundant. Sphene and other accessory minerals are present as in J75-4.

J75-8

Red coarse-grained granitic rock similar to J75-4 and J-75-7, with more abundant hornblende, and partly chloritized biotite. Also, sphene and apatite are more abundant, and often more coarse-grained, than in the above samples. Rounded grains, possibly zircon altered to a low-birefringence product, are common in biotite. Hematite alteration occurs along cracks and grain boundaries.

J75-9

Red granitic rock, somewhat finer-grained than J75-4, J75-7, and J75-8. Plagioclase is very altered; biotite is less abundant, finer-grained, and more chloritized; hornblende is also less abundant. Epidote occurs as an alteration product of plagioclase and biotite; an epidote-like mineral (allanite?) of primary origin is also present. Hematite occurs in cracks in various minerals, and in discrete grains in chlorite and in plagioclase. Accessory sphene and apatite and traces of fluorite are also present.

J75-14

Fine-grained, light-brown granitic rock with primary muscovite (minor, mostly interstitial, late crystallization), and only traces of biotite. Secondary alteration products, principally hematite and epidote, are common. These occur in clusters along grain boundaries and in cracks, and also as fillings of several parallel continuous fractures. The fractures are up to 1 mm wide, and are filled mainly with epidote (somewhat altered), and a light mineral resembling microcline with a very dusty clay alteration. Also rare grains of a pink pleochroic mineral are present.

Kloten Massif

C75-9

Fine-grained yellow, somewhat foliated granitic rock, with a pegmatitic lens parallel to the foliation. Biotite is the only mafic mineral, and it occurs sparsely as small, interstitial grains (late crystallization). Fine-grained quartz is common along grain boundaries, as is sutured quartz; thus this sample is texturally similar to Stripa quartz monzonite. Fine, very high relief, near-isotropic grains generally rounded (averaging 0.05 mm diameter), are often associated with fine cracks in quartz or feldspars. Accessory opaque grains (pyrite) are also present. Hematite alteration occurs along grain boundaries and cracks.

C75-10

Grey granitic rock with megacrysts of pink poikilitic microcline. Texture is heterogeneous, with coarse grains alternating with fine-grained intergrowths. Biotite is generally chloritized and finely intergrown with quartz. Plagioclase is commonly coarse-grained and somewhat poikilitic, with

sericite and, occasionally, chlorite alteration. Fine-grained zones appear lensoid or vein-like, and probably originate from a late-crystallizing liquid. They contain finely-intergrown quartz, feldspars, biotite-chlorite, and fluorite, usually surrounded by somewhat coarser sutured quartz. Accessory grains of an altered prismatic mafic mineral, sometimes ≥ 1 mm in length, with included epidote or zircon, are present.

C75-11

Medium- to coarse-grained foliated grey granitic rock. Feldspars and quartz are commonly coarse-grained, and mafic minerals include abundant biotite (generally fresh), lesser green hornblende, sphene, and opaque grains. The mafic minerals are usually intergrown in aggregates, with accessory fluorite (abundant), apatite and carbonate. Although locally coarse-grained, these aggregates generally have the texture of the very fine-grained elongate intergrowths of C75-10, suggesting that they are due to late stage crystallization. The altered mafic grains present in C75-10 are also found in this sample.

I 75-10

Light reddish-brown granitic rock, generally fine-grained but heterogeneous in texture and to some degree in mineralogy. Coarser lenses comprise large grains of microcline, often poikilitic and and somewhat altered, lesser coarse plagioclase grains extensively altered, and sutured quartz grains. Biotite is sparse, somewhat chloritized, and often intergrown with opaque grains. Darker lenses rich in biotite are also present in the rock. Hematite alteration occurs along grain boundaries and cracks.

I 75-11

Medium-grained, dark granitic rock, with occasional coarse micro-
cline grains. Mafic minerals are abundant, are generally intergrown in
aggregates, and include biotite (fresh), green hornblende, sphene, opaque
grains, and accessory fluorite and apatite. Locally these intergrowths grade
toward the fine, late-crystallized texture common in C75-10 and C75-11, but
typically they are much coarser-grained. Tiny grains of zircon(?) and/or
allanite(?) also occur as accessories.

I 75-22

Medium-grained granitic rock, similar to I 75-11 but lighter and more
altered. Mafic minerals are the same as in I 75-11, occurring also in aggre-
gates, and are somewhat less abundant. Alteration takes the form of partial
chlorization of biotites (which are more reddish than those of I 75-11), more
thorough alteration of feldspars, and hematite alteration in cracks.

IL 79-1

Fine- to medium-grained light yellow-brown granitic rock, texturally
heterogenous, with coarse-grained and pegmatitic lenses. Biotite is very
sparse, and is mostly chloritized; primary muscovite is present in trace
amounts. Plagioclase is extensively altered. Other alteration is similar to
that of J75-14, but to a lesser extent, and includes fine epidote and/or
hematite in cracks, and thin discontinuous clay-rich veins.

APPENDIX B. RADIOELEMENT CONTENTS, SURFACE AND UNDERGROUND MEASUREMENTS, STRIPA

Location	Rock	K (%)	U (ppm)	Th (ppm)	Th/U	Radiogenic Heat Prod. $(cal \times 10^{-13} cm^{-3} sec^{-1})$
Surface measurements, vicinity of Stripa mine						
γ-1	Leptite	3.5	3.4	10.2	3.00	4.43
γ-2	Quartz Monzonite	6.2	40.3	45.6	1.13	32.74
γ-3	Slag-Waste	–	1.6	–	–	–
γ-4 (ST-33)	SBH-2 Surface Rock	0.7	0.8	–	–	–
γ-5	Gneiss	4.0	7.5	8.9	1.19	6.78
γ-6	Leptite(?)	3.6	2.5	9.8	3.93	3.85
γ-7 (ST-1)	Leptite	3.5	3.4	11.1	3.26	4.58
γ-8 (ST-2)	Quartz Monzonite	4.4	22.0	28.0	1.27	18.59
Surface measurements on quartz monzonite, vicinity of SBH-3						
γ-57	Quartz Monzonite	3.85	26.2	29.2	1.11	21.10
γ-58 (ST-39)	Quartz Monzonite	4.1	26.9	33.1	1.23	22.27
γ-59	Quartz Monzonite	4.4	24.2	31.3	1.29	20.44
γ-60	Quartz Monzonite	4.8	28.6	38.3	1.34	24.28
γ-9 (ST-3)	Quartz Monzonite	4.1	24.7	32.7	1.32	20.89
γ-10 (ST-4)	Quartz Monzonite	4.2	22.1	27.4	1.24	18.51
γ-11 (ST-5)	Quartz Monzonite	5.2	27.1	31.8	1.17	22.42
γ-12 (ST-32)	Leptite	2.2	2.9	11.5	3.97	4.06
γ-13 (ST-38)	Leptite (?)	2.6	4.4	17.0	3.86	5.92

Appendix B (continued)

Location	Rock	K (%)	U (ppm)	Th (ppm)	Th/U	Radiogenic Heat Prod. $(cal \times 10^{-13} \ cm^{-3} sec^{-1})$
Surface measurements on granitic rocks away from Stripa						
γ-61 (ST-40)	Urgranit	4.3	6.8	22.3	3.28	8.58
γ-61a	Mica Schist (biotite)	3.6	6.1	15.7	2.57	6.95
γ-62 (ST-41)	Pinkish Urgranit	6.2	8.8	30.1	3.42	11.44
γ-63 (ST-43)	Pinkish Urgranit	5.5	7.1	25.3	3.56	9.50
γ-64 (ST-44)	Mica Schist(?) Foliated granite(?)	1.1	4.1	7.1	1.73	3.83
Surface measurements on granitic rocks away from Stripa (continued)						
γ-65 (ST-45)	Coarse granite and pegmatite	4.7	3.4	–	–	–
"	Predominantly quartz; some feldspar	1.6	4.0	–	–	–
"	Schist	2.6	7.3	11.9	1.63	6.84
Surface granite north of Gränshyttan						
γ-66 (ST-46)	Granite, fine-med. grained	5.0	40.9	36.7	0.90	31.41
γ-67 (ST-47)	Coarse-pegmatite Lt. granite	7.8	38.6	27.5	0.71	29.17
γ-68 (ST-48)	Med. grained reddish granite	4.0	14.7	28.8	1.96	14.27
Leptite north of mine area on Gullblankabanan						
γ-69 (ST-49)	Leptite	3.1	6.9	16.2	2.35	7.40
γ-70	Leptite	1.9	4.9	28.9	5.90	7.98

Appendix B (continued)

Location	Rock	K (%)	U (ppm)	Th (ppm)	Th/U	Radiogenic Heat Prod. $(cal \times 10^{-13} \, cm^{-3} sec^{-1})$
			Underground Measurements			
γ-16	Quartz Monzonite	4.0	40.9	29.4	0.72	30.02
(ST-34a sample corresponds to γ-16 series)						
γ-16a	Quartz Monzonite	3.7	33.2	28.4	0.86	25.19
γ-16b	Quartz Monzonite	3.9	36.5	28.1	0.77	27.16
γ-16c	Quartz Monzonite	3.8	34.2	30.0	0.88	26.07
γ-17a	Quartz Monzonite	3.9	42.0	28.6	0.68	30.53
γ-17b	Quartz Monzonite	4.0	40.2	29.4	0.73	29.60
γ-18	Quartz Monzonite	4.2	41.5	30.1	0.73	30.53
γ-18A	Quartz Monzonite	3.9	35.1	27.8	0.79	26.28
γ-19	Quartz Monzonite	4.0	38.5	27.5	0.71	28.28
γ-19A (ST 6,6a)	Diabase dike	2.5	6.9	11.7	1.70	6.54
γ-20	Quartz Monzonite	4.0	42.6	29.8	0.70	31.10
γ-20a (ST-18)	Chlorite-epidote mineralization at fracture intersections	3.9	45.4	33.3	0.73	33.31
γ-20b	Quartz Monzonite	4.0	40.5	31.5	0.78	30.12
γ-20c	Quartz Monzonite	3.7	41.3	30.9	0.75	30.43
γ-20d	Quartz Monzonite	3.9	39.9	30.4	0.76	29.56
γ-21	Quartz Monzonite	3.9	39.0	32.5	0.83	29.36
γ-21a	Quartz Monzonite	4.3	38.1	31.5	0.83	28.75
γ-22	Quartz Monzonite	4.2	36.3	31.5	0.87	27.65
γ-23	Quartz Monzonite	4.1	37.6	29.6	0.79	28.10
γ-24 (ST-20)	Quartz Monzonite	3.8	33.3	27.7	0.83	26.16

Appendix B (continued)

Location	Rock	K (%)	U (ppm)	Th (ppm)	Th/U	Radiogenic Heat Prod. (cal×10⁻¹³ cm⁻³sec⁻¹)
γ-25	Diabase dike	2.4	3.2	11.0	3.44	4.20
γ-26	Quartz Monzonite	3.7	39.1	32.6	0.83	29.39
γ-27 (ST-22)	Reddish Quartz Monzonite	4.2	43.4	32.6	0.75	32.07
γ-28	Quartz Monzonite	4.2	38.5	31.1	0.81	28.90
γ-29	Quartz Monzonite	4.0	36.6	29.3	0.80	27.43
γ-30	Quartz Monzonite at contact with Leptite	3.5	25.6	21.3	0.83	19.47
γ-31	Leptite at contact	3.9	13.3	17.5	1.32	11.60
γ-32 (ST-21)	Quartz Monzonite	3.6	37.0	30.1	0.81	27.71
γ-33	Quartz Monzonite	3.9	38.7	32.6	0.84	29.20
γ-34 (ST-35)	Diabase dike	2.6	7.6	13.0	1.71	7.19
γ-35	Fracture Surface on Red quartz monzonite near Leptite contact	4.4	56.5	36.5	0.65	40.56
γ-36	Leptite	3.1	4.7	20.7	4.40	6.81
γ-37 (ST-16)	Leptite, Ore with some U	2.7	33.1	11.2	0.34	22.16
γ-38 (ST-8)	Reddish Quartz Monz.	3.5	33.1	28.3	0.85	25.07
γ-39 (ST-9)	Quartz Monzonite	4.3	35.0	28.8	0.82	26.46
γ-40 (ST-10)	Quartz Monzonite	3.7	38.1	30.0	0.79	28.38
γ-41 (ST-11)	Reddish Quartz Monzonite	3.9	41.5	31.6	0.76	30.71
γ-42 (ST-12)	Quartz Monzonite	4.0	39.6	30.3	0.77	29.39
γ-43 (ST-13)	Reddish quartz monz. near leptite contact	3.5	29.1	24.2	0.83	22.03
γ-44 (ST-14,14a)	Leptite at contact	2.8	4.2	18.1	4.31	6.02
γ-45 (ST-15)	Iron Ore	2.1	3.3	9.8	2.97	4.00
γ-45A	Ore zone, Mud on floor	2.9	61.8	13.0	0.21	39.63
γ-46 (ST-17)	Pegmatite (Quartz-mica)	4.5	37.0	24.6	0.66	27.03

Appendix B (continued)

Location	Rock	K (%)	U (ppm)	Th (ppm)	Th/U	Radiogenic Heat Prod. $(cal \times 10^{-13} \, cm^{-3} sec^{-1})$
360-m Level						
γ-47 (ST-23,23a,23b)	U ore zone	3.2	85.8	17.1	0.20	54.69
γ-48 (ST-24)	Red Quartz Monzonite	3.3	31.0	24.9	0.80	23.23
γ-49 (ST-25)	Leptite	2.5	4.7	18.0	3.83	6.24
γ-50	Leptite	2.2	3.5	17.2	4.91	5.33
γ-51	Leptite	2.5	4.6	15.3	3.33	5.75
γ-52 (ST-26)	Red quartz monzonite near leptite contact	3.6	17.5	14.2	0.81	13.52
γ-53	Banded Fe Ore	2.9	3.9	14.9	3.82	5.35
γ-54 (ST-27)	Leptite	2.8	6.0	18.1	3.02	7.10
γ-55 (ST-28)	Leptite	2.6	3.9	17.7	4.54	5.74
γ-56	Leptite	2.7	3.6	18.8	5.22	5.76

APPENDIX C.   DESCRIPTION AND LOCATION OF SAMPLES PROVIDED BY
             I. LUNDSTRÖM, SWEDISH GEOLOGICAL SURVEY

SAMPLES

J 75-1

Reddish, microcline-porphyritic, homogeneous granite. The sample probably blasted by fire. No obvious signs of weathering. Loc. SW of Gussel-hyttan 11F SV/2d. Coord: 661342/146806.

L 79-1

Aplitic, red heterogeneous granite. The samples were taken approximately 30 cm below the weathering surface in a small road-cut. Loc. Small road-cut 500 m NE of Långangen, NE of Lindesberg, 11F SV/2e. Coord: 661256/147127.

J 74-1

Red, homogeneous, sparsely microcline-porphyritic granite. Cf. anal. 7594051. The sample is taken approx. 1 m below the weathering surface in a small quarry. Loc. Small quarry 450 m NE of Kallhagen, 11F SV/2d. Coord: 661000/146970.

J 75-4

Coarse, microcline-porphyritic, homogeneous granite. Cf. anal. 7594251. The sample is taken from weathering surface. Loc. 300 m W of Gäddtjärnen, 11F NV/5a. Coord: 662690/145164.

J 75-8

Coarse, more or less even-grained, homogeneous granite. Cf. anal. 7594253. The sample is taken approx. 70 cm below the weathering surface in a small road-cut. Loc. Small road-cut 100 m W of Lake Dammsjön, 11F NV/5a. Coord: 662634/145240.

J 75-9

Coarse, sparsely microcline-porphyritic granite. Cf. anal. 7594254.
The sample is taken from the weathering surface. Loc. 100 m W of Lake Gladt-
järnen, 11F NV/5a. Coord: 662741/145413.

J 75-7

Greyish, microcline-porphyritic, homogeneous granite. Cf. anal.
?594252. The sample is taken from a chunk of rock, blasted away from a
road-cut. Loc. Road-cut, 1 km SSW of Vintermossen, 11F NV/5a. Coord:
662810/145133.

J 75-14

Leuco-granite. The sample is taken from the weathering surface. Loc.
Outcrop on the southern shore of Lake Märrtjärnen, 11F NV/6a. Coord: 663160/
145193.

I 75-10

Heterogeneous leuco-granite. Cf. anal. 7594151-9. The sample is taken
from the weathering surface. Loc. Outcrop S of small Lake Bergtjärnen, 11F
NV/9c. Coord: 664580/146460.

I 75:11

Homogeneous, slightly microcline-porphyritic granite. Cf. anal.
7394305. The sample is taken approx. 20 cm below the weathering surface in a
small road-cut. Loc. Road-cut 300 m NW of Lake St. Kroktjärnen, 11F NV/8c.
Coord: 6644/0/146455.

I 75-22

Microcline-porphyritic, homogeneous granite. Cf. anal. 754308. The Sample is taken from the weathering surface. Loc. 100 m SE of small Lake Vitmosstjärn, 11F NV/8c. Coord: 664290/14625.

IL 79-1

Heterogeneous leuco-granite. Cf I 75:16, anal. 7594307. The sample is taken some dm's below the weathering surface in a small road-cut. Loc. Road-cut E of Sandsjöäsen, 11F NV/9c. Coord: 664665/146475.

C 75-9

Light, even-grained, slightly heterogeneous granite. Cf. anal. 7594353. The sample is taken from the weathering surface. Loc. 200 m W of small Lake Lisastjärn, 11F NV/7d. Cord: 663990/146835.

C 75-11

Microcline-porphyritic, homogeneous granite. Cf. anal. 7594355. The sample is taken a few dms below the weathering surface in a small road-cut. Loc. Road-cut between Lakes Blåbärstjärnen and St. Kloten, 11F NV/7d. Coord: 663782/146911.

C 75-10

Microcline-porphyritic, homogeneous granite. Cf. anal. 7594354. The sample is taken a few dm's below the weathering surface in a small road-cut. Loc. Road-cut W of the road between Lakes Kyrktjärnen and St. Kloten, 11F NV/7d. Coord: 663866/146940.